**Atmospheric
Chemistry
and Physics
Discussions**

Study of OH-initiated degradation of 2-aminoethanol

**M. Karl[1], C. Dye[1], N. Schmidbauer[1], A. Wisthaler[2], T. Mikoviny[2], B. D'Anna[3],
M. Müller[3], E. Borrás[4], E. Clemente[4], A. Muñoz[4], R. Porras[4], M. Ródenas[4],
M. Vázquez[4], and Th. Brauers[5]**

[1]Norwegian Institute for Air Research, NILU, Kjeller, Norway
[2]Institut für Ionenphysik und Angewandte Physik, Universität Innsbruck, Innsbruck, Austria
[3]IRCELYON, Institut de Recherches sur la Catalyse et l'Environnement de LYON, CNRS,
UMR5256, Université Lyon 1, Villeurbanne, France
[4]Instituto Universitario CEAM-UMH – EUPHORE, Paterna – Valencia, Spain
[5]Forschungszentrum Jülich, IEK-8 Troposphäre, Jülich, Germany

Abstract

The degradation of 2-aminoethanol (MEA) by the hydroxyl radical (OH) was studied in the European Photoreactor (EUPHORE), a large outdoor environmental chamber. High-Temperature Proton-Transfer-Reaction Mass Spectrometry (HT-PTR-MS)
and Fast Fourier Transform Infrared (FT-IR) were used to follow concentrations of reactants in the gas phase. Aerosol mass concentrations were tracked with Aerosol Mass Spectrometry (AMS). The chamber aerosol model MAFOR was applied to quantify losses of MEA to the particle phase. The rate constant k(OH+MEA) was determined relative to the rate constant of the 1,3,5-trimethylbenzene reaction with OH and was
found to be $(9.2 \pm 1.1) \times 10^{-11}$ cm^3 molecule^{-1} s^{-1}, and thus the reaction between OH radicals and MEA proceeds a factor of 2–3 faster than estimated by structure-activity relationship (SAR) methods. Main uncertainty of the relative rate determination is the unknown temporal behaviour of the loss rate of MEA to chamber wall surfaces during the sunlit experiments. Nucleation and growth of particles observed in the experiments could be reproduced by the chamber model that accounted for condensation of gaseous oxidation products, condensation of ethanolaminium nitrate and nucleation involving MEA and nitric acid.

1 Introduction

2-Aminoethanol (H$_2$NCH$_2$CH$_2$OH; MEA) is one of the most attractive absorption solvents for the removal of carbon dioxide (CO$_2$) from flue gases (Rochelle, 2009) and is regarded as industrial benchmark compound (Puxty et al., 2009; Lepaumier et al., 2009) for the CO$_2$ absorption performance in Carbon Capture Systems (CCS). Other industrial uses are mainly as corrosion inhibitor in water-based metalworking fluids (Geier et al., 2004). It is also a common ingredient of consumer products, such as detergents, degreasers, disinfectants, personal care products and pharmaceutical products (DiGuilio et al., 1992; Dow Chemicals, 2011). MEA is a natural component in

plants and animals: it is the second most abundant head group for phospholipids in cell membranes and is thus one of the most important building blocks in nature (e.g. Bakovic et al., 2007). An overview of anthropogenic and natural atmospheric sources of various aliphatic, heterocyclic and aromatic amines is given in the recent review by Ge et al. (2011a).

The use of MEA as an absorption solvent in post-combustion CO_2 capture is accompanied by losses of the amine by vaporization due to its relatively high vapour pressure of 30 Pa at 20 °C (Kapteina et al., 2005). A substance with sufficiently high vapour pressure will leave the top of the absorber column very easily together with the treated gas. MEA emissions from CO_2 capture vary strongly depending on operating conditions, for example the temperature of the absorber top. In addition, a water wash or mist eliminator installed at the top section of the absorber will substantially reduce volatility losses from the absorber. Post-combustion emissions are between 0.3 kg and 0.8 kg MEA per tonne CO_2 captured without water-wash (Goff and Rochelle, 2004), while highly efficient three-stage water-wash reduces the emissions approximately to 0.02 kg MEA per tonne CO_2 captured (Koornneef et al., 2008; Thitakamol et al., 2007). Typically, a CO_2 capture plant, that removes 1 Mt CO_2 per year from flue gas, emits between 1 ppmv and 4 ppmv MEA in the exhaust gas with single-stage water wash systems (Rao and Rubin, 2002; NVE, 2006), corresponding to about 80 t a^{-1} (Veltman et al., 2010).

Once released to the atmosphere, MEA will react during daylight mainly with the hydroxyl (OH) radical. It is known that the atmospheric oxidation of amines can lead to the formation of potentially toxic compounds such as nitrosamines, nitramines, and amides (Pitts et al., 1978; Grosjean, 1991) which are of public concern. The atmospheric oxidation of MEA with OH-radicals is initiated by H-abstraction. Abstraction of H-atoms from the −NH$_2$ group may lead to the formation of nitrosamine and nitramines. However, previous experimental studies in the European Photochemical Reactor (EU-PHORE) have shown that less than 10 % of the reaction between OH and MEA takes place at −NH$_2$ (Nielsen et al., 2011). While the nitramine of MEA, 2-nitroamino ethanol

27765

$(O_2NNHCH_2CH_2OH)$, was observed with a product yield between 0.3 % and 1.5 %, the nitrosamine of MEA, 2-nitroso amino ethanol ($ONNHCH_2CH_2OH$), was not detected (Nielsen et al., 2011). In a recent study of the environmental impact of MEA emissions from CO_2 capture, atmospheric dispersion calculations for a "worst case" situation (i.e. no degradation of MEA and its products in air, water and soil) revealed, that nitramines emitted with a fraction of only 1 % of the MEA emissions could be problematic for the aquatic environment within an area of 40×40 km^2 around a power plant equipped with CO_2 post combustion emitting 40 tonnes MEA per year (Karl et al., 2011a). To our knowledge, toxic effects of 2-nitroamino ethanol have not been studied until now. However, available data for primary and secondary N-nitro alkylamines strongly suggests that these can have mutagenic and carcinogenic effects (Goodall and Kennedy, 1976; Mirvish et al., 1980; Suzuki et al., 1985; Scherf et al., 1989; Hassel et al., 1990).

The reaction rate of 2-aminoethanol with OH has not been studied experimentally to date. This may be largely due to experimental difficulties with respect to its tendency to "stick" to Teflon (and other) surfaces and its high propensity to form aerosol particles (Carter, 2008; Nielsen et al., 2010). Estimates using structure-activity relationship (SAR) methods (Kwok and Atkinson, 1995; Meylan and Howard, 2003) indicate values in the range of 3–4 × 10^{-11} cm^3 molecule^{-1} s^{-1} for the rate constant of the OH + MEA reaction. Carter (2008) report a value of 4.4 × 10^{-11} cm^3 molecule^{-1} s^{-1} estimated using SAR and group-additivity parameters of the SAPRC-07 chemical mechanism (Carter, 2010; http://www.cert.ucr.edu/~carter/SAPRC).

Gas-phase aliphatic amines may play a significant role in secondary aerosol formation via photo-oxidation and gas-to-particle conversion in regions with high amine concentrations in air (Angelino et al., 2001; Murphy et al., 2007; Sorooshian et al., 2008; Smith et al., 2010). Aerosol particles forming in the atmospheric oxidation of amines can be either organic salt particles or non-salt particles, the latter are commonly referred to as secondary organic aerosol (SOA). Since amines are basic compounds, they can react with strong acids, commonly present in the atmosphere, such as nitric acid (HNO_3) and sulphuric acid, to form amine salts, which partition into the aerosol

27766

phase. This process can be viewed as a loss process of amines from the gas phase. However, the acid-base reaction of amines with HNO_3 is reversible and an equilibrium exists between the salt, the amine and HNO_3 (Murphy et al., 2007).

Accurate knowledge of the OH-reaction rate constant is essential for the correct prediction of atmospheric concentrations of hazardous products forming in the degradation of MEA and consequently for estimating the impact of MEA emissions from CO_2 capture on health and environment. In this study we report on experimental determination of the rate constant for the reaction of OH with MEA relative to the reaction rate constant with 1,3,5-trimethylbenzene (TMB). We also present a mechanism for atmospheric modelling the OH-initiated degradation of MEA which has been tested with chamber data obtained during a series of MEA photo-oxidation experiments.

2 Experimental

2.1 EUPHORE

Photo-oxidation experiments with MEA were carried out at the EUPHORE simulation chamber in Valencia, Spain, in the period of 26–30 July 2010. The EUPHORE facility comprises two half-spherical outdoor chambers constructed of a steel frame covered with Teflon foil, each with volume of approximately $200\,m^3$ (Becker, 1996; Vera et al., 2011; http://euphore.es/). This design has a surface/volume ratio close to one that is optimum to minimize possible losses of MEA by adsorption to the chamber walls. The experimental reactor is shielded by two retractable half-spherical protective housings which, when closed, also exclude sunlight from the reactors. To achieve homogeneous concentrations, two mixing fans are placed inside the chamber. The floor is water-cooled to minimise solar heating and the chambers are equipped with air purification and drying which provides dry air. Outside air is pressurised by means of a screw compressor to 6 bar. The compressed air is passed through a condensate trap to separate water and oil from the air and passed later through heat exchanger to reduce

27767

the absolute water content. The air is dried in absorption driers and passes a special charcoal filter to remove nitrogen oxides (NO_x), the oil vapour and non-methane hydrocarbons (NMHC). The cleaned air has the NO_x level below the detection limit of the instruments (i.e. 50 pptv), total NMHC concentration below 1 ppbv, carbon monoxide (CO) and methane are not completely removed and their concentration is at environmental level, and show high daily variability, water vapour is removed to a value <0.1 mbar, i.e. −50 °C dew point.

2.2 Instrumentation

The analysis in EUPHORE was performed using the following instrumentation:

- *O3-ML9810 (Teledyne Monitor Labs, USA).* The principle of operation of the ozone (O_3) monitor is a non dispersive ultraviolet photometer, which alternatively switches a selective ozone scrubber in and out of the measuring stream, and computes the ratio of transmitted light. A mercury vapour lamp is used as the light source (254 nm) and a solar blind vacuum photodiode is used as detector. The monitor measures O_3 with a precision of ±7 % (1-σ), accuracy of ± 2.5 % (1-σ) and has a lower detection limit of 250 pptv (1-σ).

- *NOx-ECO-ALppt 77312 (Eco Physics, Switzerland).* This monitor measures the nitrogen oxide (NO), nitrogen dioxide (NO_2) and NO_x (ppb) concentration directly from the chamber with a precision of ± 7 % (1-σ), accuracy of ± 2.5 % (1-σ) and has a lower detection limit of 50 pptv (1-σ). It has two independent units; the analyzer CLD 770 Alppt and the photolytic converter PLC 760. The principle of operation of the CLD 770 Alppt analyzer is the gas phase chemiluminescent reaction of NO with O_3. The photolytic converter PLC 760 performs a selective conversion of NO_2 to NO through photo dissociation with a xenon lamp.

- *NOx-API200AU (Teledyne Advanced Pollution Instruments Inc. USA).* This instrument measures NO_y, NO_x, NO, and NO_2 with a precision of ± 7 % (1-σ), accuracy

27768

of $\pm 2.5\%$ (1-σ) and has a lower detection limit of 70 pptv (1-σ). It measures the light intensity of the chemiluminescent gas phase reaction of NO with O_3. The analyzer samples the gas stream and measures the NO concentration by digitizing the signal from the analyzer's photomultiplier tube (PMT). A valve then routes the sample stream through a converter containing heated molybdenum to reduce any NO_x present to NO at 315 °C. Then the analyzer measures the total NO_x concentration. The NO_x and NO values are subtracted from each other to obtain the NO_2 concentration.

– *J(NO_2) Filter Radiometer (Meteorologie Consult GmbH, Glasshütten, Germany).* The filter radiometer is installed inside the Teflon chamber, 50 cm above the chamber floor, to measure the NO_2 photolysis frequency. The field of view is 2×180 degrees (4πsr). Wavelength characteristics are obtained from best fit to the photolysis frequency of the NO_2 molecule. Absolute calibration is better than $\pm 5\%$ with respect to a chemical actinometer and linearity is better than 1 % according to the detector characteristics.

– *High-Temperature Proton-Transfer-Reaction Mass Spectrometer (HT-PTR-MS).* A HT-PTR-MS (Mikoviny et al., 2010) was used for high time resolution measurements of MEA and 1,3,5-trimethylbenzene. Sample-wetted surfaces of the HT-PTR-MS were kept at 200 °C to minimize adsorption and desorption effects of MEA. Previous work has shown that the $1\,e^{-2}$ response time of the HT-PTR-MS to MEA is in the 5-to-18 s range (Mikoviny et al., 2010). The HT-PTR-MS was interfaced to the EUPHORE chamber via a Sulfinert® passivated stainless steel tube (length: 125 cm, i.d.: 5.33 mm; temperature: 230 °C; flow: 10 slpm). Instrumental sensitivity for 1,3,5-trimethylbenzene was determined experimentally using a certified gas standard (AiR, Denver, USA). MEA quantification was based on calculated proton transfer reaction rate coefficients (Nielsen et al., 2010). Detection limit of TMB and MEA with the HT-PTR-MS is 100 pptv (Mikoviny et al., 2010). Both compounds can be measured with a 1-σ precision of $\pm 10\%$ or better. The

27769

1-σ accuracy is estimated to be $\pm 10\%$ for TMB and $\pm 15\%$ for MEA.

– *Fast Fourier Transform Infrared (FT-IR) Spectroscopy.* The spectrometer (NICOLET 6700, MCT-detector) is coupled to a long-path multi-reflection cell installed in the chamber for the detection in the IR spectral range (650–4000 cm^{-1}). The gold-coated mirrors of the cell allow a total path length of 554 m. Spectra are collected with resolution 1 cm^{-1} by averaging 280 scans, resulting in a sampling time of 5 min per spectrum. Concentrations of sulphur hexafluoride (SF_6), MEA, and formamide (H_2NCHO) during the experiments were determined with improved analysis software developed at CEAM (Ródenas, 2008) by analysing the IR spectra using calibrated reference spectra collected a priori. Typical detection limits for the analyzed compounds are a few ppb. Accuracy (1-σ) is $\pm 10\%$ for formamide and SF_6. The quantification of MEA was done by cross-calibration against MEA measurements of the HT-PTR-MS instrument with an estimated accuracy of about $\pm 15\%$.

– *Gas chromatography with photo ionisation detector (GC-PID).* The GC-PID operated using a 30 m DB-624 fused silica capillary column (J&W Scientific, 0.32 mm i.d., 1.8 mm film). Air was sampled from the chamber into a 3 cm^3 sampling loop and then injected onto the column. The column was maintained at a constant temperature (120 °C). The GC-PID analyzed TMB with a precision of $\pm 10\%$ (1-σ), accuracy of $\pm 10\%$ (1-σ) and detection limit of 0.6 ppbv.

– *PTR-TOF 8000 Proton-Transfer-Reaction Time-of-Flight Mass Spectrometer.* A commercial PTR-TOF 8000 (Ionicon Analytik GmbH, Innsbruck, Austria) was used to measure formamide (Jordan et al., 2009). With a mass resolving power $m/\Delta m$ of ≈ 3000 (FWHM), the PTR-TOF specifically detects formamide in its protonated form at a mass-to-charge ratio (m/z) 46.02874. Nitric acid which is typically produced in high NO_x smog chambers experiments is detected separately at m/z 45.9923 ($H_3O^+ + HNO_3 \rightarrow NO_2^+ + H_2O + H_2O$). PTR-MS instruments with quadrupole mass filters (e.g. the HT-PTR-MS) detect both species at m/z 46.

27770

The PTR-TOF was only used for formamide measurements here, because its time response for MEA was too slow for kinetic measurements. The PTR-TOF-MS was interfaced to the chamber via a PEEK capillary tube (length: 220 cm, i.d.: 1.01 mm; temperature: 160 °C; flow: 0.5 slpm). Formamide quantification was based on calculated proton transfer reaction rate coefficients (Nielsen et al., 2010).

– *Compact Time-of-Flight Aerosol Mass Spectrometer (c-TOF AMS).* The c-TOF AMS (Drewnick et al., 2005) was employed to characterize the chemical composition of non refractory aerosols. The AMS utilizes thermal flash evaporation of the aerosol followed by electron impact ionization and ion detection by TOF-MS. Measured ions are analyzed using the high resolution data analysis methods described by Müller et al. (2011) and are grouped into chemical species (organics, nitrates, ammonium, sulphates). For quantification, calibrations using ammonium nitrate, ammonium sulphate and MEA nitrate have been performed.

– *Tapered Element Oscillating Monitor (TEOM) model 1400a (Ruppercht and Patashnick Co. Inc, Albany, USA).* This instrument measures aerosol mass concentration with a 1 min scan rate. The particles were collected on a replaceable 0.5 cm diameter filter, which was mounted on an oscillating microbalance, with a sampling flow of $3 \, l \, min^{-1}$, at 27 °C.

– *Scanning Mobility Particle Sizer (SMPS), model 3080 (TSI Incorporated, Shoreview, USA).* Particle measurements were also made with a SMPS system that consists of a differential mobility analyzer, model 3081, and a condensation particle counter, model 3022A, which measure size distributions in the 11–982 nm diameter range in real time with a 5 min scan rate. Sheath and aerosol sampling flows were $2 \, l \, min^{-1}$ and $0.30 \, l \, min^{-1}$, respectively.
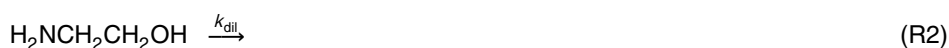
27771

2.3 Experiments

Two experiments were performed on the relative determination of the rate constant (E1 and E2) and one experiment was performed to test the mechanism for OH-initiated atmospheric degradation of MEA (E3). Various amounts of NO and NO_2, 400 µl MEA, and a known amount of TMB (only in E1 and E2) were injected into the dark chamber and after approximately one hour the canopy of the chamber was opened and the mixture was exposed to sunlight. Initial mixing ratio of TMB in E1 and E2 was about 200 ppbv. MEA was injected with a Harvard 22 syringe pump system with air stream heating (Fournier et al., 2008; with modifications) which allows for transfer of a known amount of MEA into the chamber. However, MEA losses during injection which occur between the outlet of the syringe and the inlet of the chamber can be substantial and it was not possible to quantify the lost amount. The quantification of MEA mixing ratios in the chamber air relied on measurements with the HT-PTR-MS and FT-IR instruments. Maximum MEA mixing ratios were reached about 15 min after start of the injection. Ranges of O_3, NO and NO_2 concentrations in experiments E1–E3 are presented in Table 1 together with average relative humidity (RH) and temperature (T). Time series of O_3, NO, NO_2 and the photolysis frequency of NO_2, $j(NO_2)$, during E1 and E2 are shown in Fig. 1.

3 Chamber model description and mechanism

In the chamber, MEA is subject to the following loss processes:

$$H_2NCH_2CH_2OH + OH \xrightarrow{k_1} products \tag{R1}$$

$$H_2NCH_2CH_2OH \xrightarrow{k_{dil}} \tag{R2}$$

$$H_2NCH_2CH_2OH \xrightarrow{k_{wall}} \tag{R3}$$

27772

$$H_2NCH_2CH_2OH + HNO_3 \xleftrightarrow{K_p} H_3NCH_2CH_2OHNO_3(s) \qquad \text{(R4)}$$

The aim of this study is to determine the rate constant k_1 of Reaction (R1) between MEA and OH radicals. During the experiments, all compounds are diluted by the replenishment flow. The replenishment flow is added to ensure a constant chamber volume by replacing air that is lost due to outtake by the connected instruments and through the Teflon foil. The first order loss rate constant k_{dil} for dilution was determined from the first order decay of SF_6 gas during the experiments. The loss of MEA to chamber walls can be described as a first order loss. The first order loss rate k_{wall} was determined in our study from the decay of MEA in the period after injection of MEA into the dark chamber starting at the time when homogeneous distribution in the chamber volume was reached until the time of opening the canopy. MEA reacts in thermodynamic solid-gas equilibrium with HNO_3 to form solid aminium nitrate (Reaction R4) which partitions to the aerosol phase. A detailed chamber aerosol model has been used to derive the rate for the loss of MEA to particles, $k_{particles}$, as function of time (see Sects. 3.5 and 3.6).

3.1 Model description

Modelling of chamber experiments was done using the multicomponent aerosol dynamics model MAFOR (Marine Aerosol Formation model) version 1.3 which includes gas phase and aqueous phase chemistry in addition to aerosol dynamics (Karl et al., 2011b). In MAFOR, the general dynamic equation of the aerosol is solved using a sectional approach with a fixed grid. Mass transfer of gas molecules to particles is calculated using the Analytical Predictor of Condensation scheme (Jacobson, 1997). The various aerosol dynamical processes are treated by calculation of the particle number concentration and component mass concentrations of each size section as functions of time. The number of size sections can be selected by the user; in this study 100 size bins were used to represent the aerosol size distribution ranging from 1 nm to 10 μm diameter sizes.

The detailed gas phase chemistry scheme of the model based on the Module Efficient Calculating the Chemistry of the Atmosphere (MECCA) (Sander et al., 2005; Sander et al., 2011) includes chemistry of C2–C4 alkanes, propene, isoprene and dimethyl sulphide (Karl et al., 2007). For the purpose of this study, a chemistry mechanism for the OH-initiated oxidation of MEA (described in Sect. 3.3) and a simple scheme for TMB were added (Table 2). A simplified treatment of the TMB chemistry is considered to be adequate since it is not intended to model concentrations of TMB oxidation products in this study. Photolysis frequencies are calculated using the method of Landgraf and Crutzen (1998) and data on absorption coefficients and quantum yields recommended by the Jet Propulsion Laboratory (JPL) Evaluation no. 15 (Sander et al., 2006).

The current mechanism of MAFOR v1.3 contains 383 reactions and 221 compounds in the gas phase. The kinetic pre-processor (KPP; http://people.cs.vt.edu/~asandu/Software/Kpp/) solver package is used to generate Fortran95 code for the chemistry module and the Rosenbrock 3 solver is used for integration the differential equation system of gas phase reactions (Sandu et al., 1997; Sandu and Sander, 2006). Change of number and mass concentration of particles is solved subsequent to the integration of the gas phase/liquid phase chemistry.

3.2 Chamber sources and losses

Parameterizations of the chamber wall sources of nitrous acid (HONO), S_{HONO}, and formaldehyde (HCHO) are included in the model. The photolysis of HONO in sunlight was the main source of OH during the experiments in EUPHORE. The HONO wall source is parameterized as function of $j(NO_2)$, temperature and relative humidity for dry and humid conditions (Zádor et al., 2006). The light-dependent source of formaldehyde (Zádor et al., 2006) is used in the model. First order wall loss rates for O_3, NO_2 and HNO_3 of $3 \times 10^{-6}\,s^{-1}$, $1.15 \times 10^{-5}\,s^{-1}$ and $8.2 \times 10^{-5}\,s^{-1}$, respectively, and a OH-to-HO_2 conversion rate of $8.4\,s^{-1}$ to account for the background reactivity of the chamber

(Bloss et al., 2005a), have been used in the simulation of experiments. Loss rates for O_3 and NO_2 were not relevant in our study because monitored time series of NO_2 and O_3 concentrations were used as model input in simulations of the experiments. Further, measured time series of NO concentrations, temperature and $j(NO_2)$ were used to constrain the model. A size-dependent parameterization of the wall loss of particles in the chamber is included in the model to reproduce the particle loss. The parameterization is according to Naumann (2003) and takes into account the geometry of the EUPHORE chamber.

3.3 Atmospheric mechanism for the OH-initiated degradation of MEA

The mechanism for the OH-initiated oxidation of MEA used in the model simulations is provided in Table 3. The mechanism has been constructed during the project ADA-2009 ("Atmospheric Degradation of Amines, 2009"; Nielsen et al., 2010), based on quantum chemical calculations (Bråten et al., 2008), SAR estimated rate constants and adjusted to fit experimental data in MEA photo-oxidation experiments in EUPHORE. The scheme contains 15 reactions and 17 compounds in the gas phase.

According to Nielsen et al. (2011), the formation of the following products was unambiguously attributed to the OH-initiated oxidation of MEA in the EUPHORE experiments: formaldehyde (HCHO), formamide (H_2NCHO), amino acetaldehyde (H_2NCH_2CHO), 2-oxo-acetamide ($H_2NC(O)CHO$), 2-imino ethanol ($HN=CHCH_2OH$) and the 2-nitroamino ethanol (for more details it is referred to Table 1 in the publication by Nielsen et al., 2011). The OH + MEA mechanism presented in Table 3 includes reaction pathways leading to the formation of all these compounds. In addition to the schematic gas phase degradation routes outlined by Nielsen et al. (2011), kinetic and mechanistic information about the degradation of the major oxidation product, i.e. formamide, provided by Barnes et al. (2010) was taken into account. Average branching ratios of the initial H-abstraction given by Nielsen et al. (2011) are 8 % from $-NH_2$, 84 % from $-CH_2-$ and 8 % from $-CH_2OH$. In our presented mechanism, the branching ratios were slightly modified and are 15 %, 80 %, and 5 % for the $-NH_2$, $-CH_2-$,
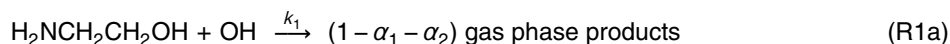
and $-CH_2OH$ positions, respectively. These branching ratios have been used in model simulations of EUPHORE experiments in the report by Nielsen et al. (2010) and resulting gas phase concentrations of formamide and 2-nitroamino ethanol were in agreement with measured concentrations of these compounds by PTR-TOF-MS within the uncertainty of measured data.

EPI Suite™ version 4.0 (U.S. EPA, 2009) has been used to estimate rate constant for reactions with the OH radical in case no experimental data was available. The Atkinson method is implemented in the program EPI Suite™ through the module AOP-WIN. AOPWIN incorporates updated fragment and reaction values as given by Kwok and Atkinson (1995). In addition, Syracuse Research Corporation has added additional fragment and reaction values from more recent experimental data (Meylan and Howard, 2000). The accuracy of the method has been evaluated in a test of 720 chemicals with respect to the non-logarithmic rate constant values: 90 % of the predicted values were within a factor 2 of experimental data and 95 % within a factor 3 (Meylan and Howard, 2003). Unfortunately, Atkinson's method has shown larger deviations for several important classes of chemical compounds such as organic compounds with 3 halogens on the same carbon atom (as in DDT), chemicals with NO_x-groups as in nitroalkanes, phosphates, often used in herbicides, and small heterocyclic rings (Güsten, 1999).

3.4 SOA formation in the OH-initiated oxidation of MEA

MAFOR uses a hybrid method of condensation and partitioning to treat formation of SOA from the OH-initiated oxidation of MEA. Since the specific condensing oxidation products that form in the photo-oxidation of MEA are only tentatively known (Nielsen et al., 2011), the model uses a simplified approach of two semi-volatile products ("two-product model"), one less volatile and one more volatile condensing compound, that can partition to an absorptive organic aerosol phase (Odum et al., 1996; 1997). The two products, termed MEAp1 and MEAp2, are formed in the initial reaction of MEA and OH (Reactions R1b and R1c below) with the molar stoichiometric yield α_1 and α_2, respectively, (see Table 4):

$$H_2NCH_2CH_2OH + OH \xrightarrow{k_1} (1 - \alpha_1 - \alpha_2) \text{ gas phase products} \tag{R1a}$$

$$H_2NCH_2CH_2OH + OH \xrightarrow{k_1} \alpha_1 \text{ MEAp1} \tag{R1b}$$

$$H_2NCH_2CH_2OH + OH \xrightarrow{k_1} \alpha_2 \text{ MEAp2} \tag{R1c}$$

The equilibrium partitioning of the two condensable compounds between the gas phase and the aerosol phase is described by the gas/particle partitioning coefficient for absorptive uptake into the particle phase (e.g. Seinfeld and Pankow, 2003). An ideal solution was assumed between the dissolved species (MEAp1 and MEAp2), and the other components of the (organic) particulate phase.

The SOA yield from OH-initiated oxidation was determined in experiments E4 and E5 (Table 1) as the ratio of the amount of MEA reacted (ΔMEA_{reac}) to the total mass concentration of organic aerosol (ΔM_o). The time series of reacted ΔMEA_{reac} was derived from a model simulation with MAFOR and time synchronized to the time series of ΔM_o measured by AMS. SOA yields, Y^{SOA}, were calculated for each AMS data point in E4 and for the final AMS data point in E5 ($Y^{SOA} = \Delta M_o / \Delta MEA_{reac}$). Mass-based stoichiometric yields for MEA were fit to the experimental yield data, assuming a two-product model, by using a modified Marquardt-Levenberg parameter estimation method (Fahlman, 2001). Parameters resulting from the fit to the yield curve (Fig. 2) are provided in Table 4. Based on the data it is difficult to decide whether a one-product or a two-product model is more adequate. A two-product model was chosen because it offers more flexibility to take into account dependencies of SOA yields on other variables such as the VOC/NO$_x$ ratio. Due to the limited number of experiments it is currently not possible to deduce a NO$_x$-dependence of SOA yields from the OH-initiated oxidation of MEA. It is noted that gas phase losses of MEAp1 and MEAp2 to the chamber walls were not considered in this study.

In the photo-oxidation of 1,3,5-trimethylbenzene mass-based aerosol yields of ranging from 3.4 to 8.1 % have been found in experiments without seed particles present

27777

(Cocker et al., 2001). Based on this a molar-based SOA yield of 4 % in the reaction of OH with TMB was assumed in the model calculations of this study.

3.5 MEA losses to particles

The mass balance of MEA considering losses through Reactions (R1–R4):

$$\frac{d[MEA]}{dt} = L_{MEA} + \left(\frac{d[MEA]}{dt}\right)_{particles} + \left(\frac{d[MEA]}{dt}\right)_{\rho} \tag{1}$$

Here the squared brackets denote gas phase concentrations (in molecules cm^{-3}). The first term on the right hand side (RHS) of Eq. (1), L_{MEA}, is the total gas phase pseudo first order loss rate:

$$L_{MEA} = -(k_1[OH] + k_{dil} + k_{wall})[MEA] \tag{2}$$

The second term on the right hand side of Eq. (1) accounts for concentration changes due to formation of amine salts that partition to the aerosol phase and the third term considers concentration changes due to changes of density of air, ρ, caused by the daily cycle of pressure and temperature. MEA concentration changes with time due to transfer to/from particles are predicted by:

$$\left(\frac{d[MEA]}{dt}\right)_{particles} = -2\pi D \sum_{k=1}^{N_B} N_k d_{p,k} f(Kn, \alpha_m) \times ([MEA] - [MEA]^{eq}) - J_{nucl} \upsilon_{MEA} \tag{3}$$

The first term on RHS of Eq. (3), describes concentration changes due to mass transfer of the ethanolaminium nitrate produced in Reaction (R4) to a particle population. The second term on RHS considers loss of MEA due to nucleation of MEA-HNO$_3$

27778

clusters. In Eq. (3), N_k is the number concentration of particles in size bin k, (with N_B being the number of size bins), $f(Kn, \alpha_m)$ is the correction for non-continuum effects and imperfect accommodation as defined by Fuchs and Sutugin (1970), Kn is the Knudsen number, D is the gas phase diffusion coefficient, $d_{p,k}$ the diameter of particles in size bin k, υ_{MEA} is the volume ratio (ratio of the volume of a MEA molecule to the volume of a particle in the first size bin). The accommodation coefficient α_m for the mass transfer of ethanolaminium nitrate to particles was assumed to equal unity.

The equilibrium concentration of MEA, $[MEA]^{eq}$, in the MEA-HNO$_3$ system is defined in analogy to the ammonia-nitric acid system, by (Seinfeld and Pandis, 1998):

$$[MEA]^{eq} = \left(\frac{[MEA] + [HNO_3]}{2} \right) + \sqrt{\frac{([MEA] - [HNO_3])^2}{4} + K_p'} \qquad (4)$$

The dissociation constant, K_p' in units (molecules cm^{-3})^2, for ethanolaminium nitrate can be defined as product of the equilibrium concentrations of MEA and HNO$_3$ (Seinfeld and Pandis, 1998):

$$K_p' = K_p / (RT)^2 = [MEA]^{eq} \times [HNO_3]^{eq} \qquad (5)$$

Formation of the ethanolaminium nitrate salt according to (R4) is limited by the availability of the least abundant of the two species. Any excess of MEA may then react with HNO$_3$ to form the ethanolaminium nitrate. Ge et al. (2011b) estimated dissociation constants of several aminium nitrate salts in the temperature range 263.15-323.15 K. The dissociation constant of ethanolaminium nitrate is given by $K_p' = 8 \times 10^{16}$ (molecules cm^{-3})^2 at 293.15 K (Ge et al., 2011b) and this value was used for the modelling of the experiments in our study.

It is assumed in this work that nucleation observed in MEA oxidation experiments occurs through homogenous heteromolecular nucleation between HNO$_3$ and MEA

vapour molecules, or one of the vapours activating the clusters composed around a molecule of the other vapour. The parameterization for the nucleation process developed in this work is:

$$
\begin{aligned}
J_{nucl} &= K_{nucl} \times [MEA] \times [HNO_3] & [MEA] \times [HNO_3] > K_p' \\
J_{nucl} &= 0 & [MEA] \times [HNO_3] \le K_p'
\end{aligned} \qquad (6)
$$

According to this parameterization, nucleation can only happen when the product of HNO$_3$ and MEA concentrations exceeds a threshold of K_p'. K_{nucl} is an empiric nucleation parameter. An average nucleation parameter is given by $K_{nucl} = 2 \times 10^{-20}$ cm^3 molecules^{-1} s^{-1}, as determined by fitting the temporal evolution of number size distributions during MEA experiments in EUPHORE (Nielsen et al., 2010), and was used for the modelling of the experiments in our study.

3.6 Model simulation of chamber experiments

The loss of MEA to the aerosol phase in the experiments competes with the gas phase reaction between OH and MEA. For the determination of the rate constant between OH and MEA in this work an estimate of the net loss rate of MEA to particles is required. To this end, Eq. (3) is expressed as net loss of MEA to the aerosol phase of the form:

$$\left(\frac{d[MEA]}{dt} \right)_{particles} = -k_{particles}[MEA] \qquad (7)$$

with

$$k_{particles} = 2\pi D \sum_{k=1}^{N_B} N_k d_{p,k} f(Kn, \alpha_m) \times \left(1 - \frac{[MEA]^{eq}}{[MEA]} \right) + J_{nucl} \upsilon_{MEA}[MEA]^{-1}$$

where $k_{particles}$ is a quasi first order loss rate constant. Since $k_{particles}$ depends on the actual MEA equilibrium concentration (see Eq. 4), it is not possible to determine it directly from measured concentrations of particle numbers. MAFOR is used in this study to compute $k_{particles}$ as function of time in each experiment. The model included the atmospheric mechanism of OH+MEA (Sect. 3.3); SOA formation (Sect. 3.4) was taken into account in addition to the formation of ethanolaminium nitrate salt (Sect. 3.5). Gas phase concentrations of HONO and HNO_3 were not monitored in the chamber experiments. However, FT-IR signal indicates that HNO_3 concentrations were below the detection limit of 2 ppbv during the experiments. In the model calculations, the only adjusted parameters are the start concentration of HONO and the chamber wall source of HONO, which affect both the OH concentration and NO_x available for the formation of the ethanolaminium nitrate salt. A factor F_{source} was used to scale the chamber wall source of HONO (S_{HONO}):

$$S_{HONO}^{fit} = F_{source} \times S_{HONO} \tag{8}$$

The fit procedure proceeded until best agreement between modelled and monitored time series of total and nitrate particle mass concentrations (as measured by AMS) and of MEA gas phase concentrations as well as of TMB gas phase concentrations (in case TMB was present) had been achieved. Comparison of AMS nitrate signals obtained during the experiments with the nitrate signal of the pure ethanolaminium nitrate (reference) salt revealed that about 85 % of the total nitrate concentrations observed in the experiments of this study could be attributed to ethanolaminium nitrate salt.

4 Relative rate

For the chamber experiments, the balance equations of MEA, TMB and SF_6 can be written as a set of first order ordinary differential equations:

$$\left(\frac{d<MEA>}{dt}\right) = -\left(k_1[OH] + k_{dil} + k_{wall} + k_{particles}\right) <MEA>$$

$$\left(\frac{d<TMB>}{dt}\right) = -(k_{ref}[OH] + k_{dil}) <TMB>$$

$$\left(\frac{d<SF_6>}{dt}\right) = -k_{dil} <SF_6> \tag{9}$$

We note that the density dependent term vanishes when mixing ratio (denoted by $<\ >$), is used instead of concentration. After integration and rearrangement of the set of balance equations, see Eq. (A1–A10) in the Appendix A, it is possible to derive a standard relative rate equation:

$$Y'_{MEA}(t) = \frac{k_1}{k_{ref}} X'_{TMB}(t) \tag{10}$$

A linear least-squares-model (LSQ) is invoked by

$$Y'_{MEA}(t) = a + b \cdot X'_{TMB}(t) \tag{11}$$

where the slope b corresponds to the ratio k_1/k_{ref} and a is the offset from zero of the y-axis. The reference rate constant k_{ref} for the OH+TMB reaction is taken from Aschmann et al. (2006), with the temperature dependent expression: $k_{ref}(T) = 4.40 \times 10^{-12} \exp(738 \pm 176/T)$.

5 Results

The time series for the pseudo first order loss processes were time synchronized onto the HT-PTR-MS time grid before use in the LSQ model. Only the first 1300 s of the

respective sunlit experiment were analyzed with the LSQ model. For each experiment, the first order loss rate constants and their associated uncertainties were determined (average and standard deviation in Table 5). The time-dependent dilution loss term $D_{SF_6}(t)$ (defined by Eq. (A6)) was derived from the measured SF_6 time series. The time-dependent loss rate of MEA to particles, $k_{particles}$, was determined by the chamber aerosol model according to Eq. (7), as described in Sect. 3.6. Modelled time series of total aerosol mass concentrations obtained in the fit procedure are in excellent agreement with the total mass concentration measured by AMS (Fig. 3).

The lifetime of MEA towards dilution, wall loss and loss to particles ranged between 8–11 h, 1–2 h and 40–60 h, respectively. Thus, loss of MEA to particles was the least sensitive parameter in the LSQ for determination of the rate constant k_1.

Linear regression which takes into account errors in both X' and Y' was applied and a regression routine based on FITEXY.C (Press et al., 1992) was used. This regression method usually provides a better estimate of the true value of the slope (k_1/k_{ref}) and of the intercept than a simple regression analysis which does not take the errors of the measured concentrations of both reactants into account (Brauers and Finlayson-Pitts, 1997). Results of the LSQ for experiment E1 and E2 are shown in Fig. 4 and the corresponding values for a and b are given in Table 6. X' and Y' were found to be highly correlated, correlation coefficients were $R^2 = 0.981$ in E1 and $R^2 = 0.992$ in E2. The merit function χ^2 provides a means for the "goodness of fit" of the data to the invoked linear model (Press et al., 1992). In both experiments the probability that χ^2 exceeds a particular value by chance was $Q = 1$ in the regression analysis, supporting the adequateness of the linear LSQ model.

Further the validity of the LSQ model was tested in Monte Carlo (MC) simulations where the time series $X'(TMB, t)$ and $Y'(MEA, t)$ were shifted randomly according to the standard deviation of the MEA and TMB measurements and of the loss terms (with $M = 10\,000$ repetitions). It is noted that the values of a and b and their variance (1-σ standard deviation of the mean) resulting from MC analysis were not significantly different from the values obtained in the LSQ fit.

27783

A slight curvature of the data can however be noted in Fig. 4 for the data points in both experiments. During the first 3–5 min of the relative rate experiment, data points seem to follow the unity slope (grey dashed 1:1 line) while the later data points are all on a line with a slope greater unity as it is indicated by the LSQ model. A reason for the obvious curvature could be that the loss processes other than OH-reaction were not correctly subtracted when calculating Y' (Eq. A9) or that these loss processes are time-dependent. When a longer time period of the experiments, for instance 2600 s, is considered, the LSQ model resulted a slope >2. This could indicate that there is a loss process that increases over time during the sunlit experiment. While the time-dependence of the dilution loss and the particle loss terms can be accurately estimated, the time behaviour of the wall loss term is unknown. A more detailed discussion of the wall loss follows in Sect. 6.1.

Based on the results from the LSQ model, the rate constant k_1 of the reaction between OH and MEA is found to be $(9.3 \pm 1.0) \times 10^{-11}$ cm^3 molecule^{-1} s^{-1} in experiment E1 (average temp. 303.6 ± 0.4 K) and $(8.1 \pm 0.8) \times 10^{-11}$ cm^3 molecule^{-1} s^{-1} in E2 (average temperature 306.6 ± 1.4 K). The average rate constant from the two experiments, extrapolated to 298 K using the temperature dependence of k_{ref}, is $(9.2 \pm 1.1) \times 10^{-11}$ cm^3 molecule^{-1} s^{-1}. This experimentally derived value is a factor of 2.6 higher than the value of 3.58×10^{-11} cm^3 molecule^{-1} s^{-1} predicted by EPI Suite v4.0 which makes use of the Atkinson SAR (Table 6).

With the intention to study the sensitivity of the coupled gas-phase/aerosol chemistry system on sudden changes of the VOC/NO$_x$ regime, experiment E2 was perturbed by the injection of 12 ml NO at 14:42 UTC, about 1 h after opening the canopy (Fig. 1b). The primary effect of the NO injection was to increase ozone production (ozone mixing ratio increased by 40 ppbv) and by this to increase OH-reactivity, causing pronounced changes of measured decay rates of MEA and TMB (HT-PTR-MS data, Fig. 3b). The secondary effect was to increase production of gaseous HNO$_3$ through the OH + NO$_2$ reaction potentially causing more particle-bound nitrate to be formed. The total aerosol mass concentration increased by 70 µg m^{-3}. According to the simulation with MAFOR,

27784

the observed aerosol mass increase was mainly due to increase of nitrate. MAFOR predicts slightly faster MEA decay compared to HT-PTR-MS.

In further simulations with MAFOR the effect of the higher $k(OH + MEA)$ value found in this work on the predicted concentrations of gaseous oxidation products was investigated. Experiment E3 was modelled in the same way as described in Sect. 3.6, by scaling the rate constant value of $k_1 = 3.58 \times 10^{-11}$ cm^3 molecule^{-1} s^{-1} by a factor of 2.6, and fitting the model output towards measured MEA mixing ratios and aerosol mass concentrations (Fig. 5).

A molar yield of 0.55 instead of 0.33 had to be used for MEAp1 in order to match the measured aerosol mass in E3. Modelled formamide mixing ratios were found to agree very well with those measured by FT-IR, while overestimating those measured by PTR-TOF-MS. MAFOR predicts 2-nitroamino ethanol concentrations of up to 3 ppbv in E3. The product yield of the nitramine is estimated to be 0.75 %, which is within the range of experimental product yields of 0.3 % to 1.5 % found by Nielsen et al. (2011) in experiments with various NO$_x$-levels.

By repeating the simulation with the original value of k_1 and comparing the modelled time series, it was found that steady state concentrations of 2-nitroamino ethanol and formamide in the experiment increased by 39 % and 36 %, respectively, when applying the higher k_1 value.

6 Discussion

6.1 Rate constant uncertainties

It was assumed that the wall loss rate of MEA was the same in the sunlit experiment as in the dark period before opening the canopy. During the experiment, the chamber walls are heated by the sun which could cause desorption of MEA from the Teflon surface, leading to smaller wall loss rates. On the contrary, heating of the chamber floor by the sun may cause convective movement of air inside the chamber which would

27785

cause a more rapid loss of MEA to the Teflon walls. As noted before, the curvature of the relative rate data indicates a loss rate that increases over time during the sunlit experiment. It can be speculated that the temperature of the floor increased during the sunlit experiment (despite the floor cooling) and consequently accelerated the convective movement. However, we note that mixing of the chamber air by the powerful fan system will introduce a much stronger movement of air than the thermally induced convection does. Mixing by the fans is expected to result in a constant loss of MEA to the Teflon walls.

We assume that there was a high short-term variability after the opening of the chamber canopy which introduced large errors to the first measured data points of the sunlit experiment. To estimate the influence of wall loss changes on our result, the LSQ fit was repeated with ±50 % higher and lower wall loss rates. As a result $k(OH + MEA)$ varied by ±24 %. In a second test the wall loss rate was increased linearly over time until it reached a 50 % higher value at the end of the selected time period of 1300 s. This resulted in a decrease of the slope b by 22 %. It is emphasized that the experimentally derived k_{wall} before and after the sunlit experiments never showed larger variations than given by the standard deviation (ca. ±35 %, see Table 5).

It can be speculated that there was a competing reaction of NO$_3$ radicals with MEA during the experiments. Experiments were performed under full sunlight and NO$_3$ undergoes rapid photolysis under such conditions. Modelled NO$_3$ concentrations were highest at the start of the experiments with a maximum value of 4×10^7 radicals cm^{-3}, while modelled OH concentrations were $\approx 5 \times 10^6$ radicals cm^{-3}. The rate constant of the reaction NO$_3$ + MEA is not known from experiments and EPI Suite currently offers no possibility to estimate rate constants of NO$_3$-reactions. Using the new quantitative structure-property relationship (QSPR) for NO$_3$-degradation of VOC given by Papa and Gramatica (2008), the molecular descriptors HOMO (highest occupied molecular orbital) computed with the molecular modelling software CAChe system (2000–2005 Fujitsu Limited) using semi empirical quantum mechanics (MOPAC PM3), and Me (mean atomic electronegativity of Sanderson) computed by DRAGON software

27786

version 6 (Todeschini et al., 2011), a value of 1.48×10^{-13} cm^3 molecule^{-1} s^{-1} was calculated for this rate constant (E. S. Heimstad, personal communication, 2011). Using this value, the NO$_3$ + MEA reaction is estimated to contribute less than 4 % to the overall decay of MEA.

The error of the model-derived particle loss rate, $k_{particles}$, is estimated to be ±15 % due to the instrumental error of AMS and the error of the nitrate signal. The loss of MEA to particles has been found to be a minor contribution (<4 %) to the overall loss of MEA during the kinetic experiments.

The only other temperature-dependent rate data for the reaction of OH radicals with TMB is published by Geiger et al. (2002). For the temperature range of 278–320 K their expression is $k_{ref} = 6.3 \times 10^{-12} \exp(670/T)$ (Geiger et al., 2002; Aschmann et al., 2006). Rate constants calculated using this expression are uniformly higher by 11–15 % over the temperature range 278–320 K than those calculated using the expression by Aschmann et al. (2006). In our data analysis, the use of the expression by Geiger et al. (2002) would imply a higher rate constant for the reaction of OH with MEA, by 14 % and 15 % in experiment E1 and E2, respectively.

Using the LSQ model with the MEA mixing ratio measured by FT-IR (time-synchronized on the PTR-MS grid) instead of the HT-PTR-MS data resulted in a 9 % and 30 % lower rate constant estimate in E1 and E2, respectively. However, the MEA time series from FT-IR are less accurate because of the possible presence of unknown compounds that absorb in the same spectral region as MEA. Figure 3a and 3b show that there were no systematic discrepancies for the MEA measurement by both instruments, but the time series show different slopes, in particular when mixing ratios are small.

Systematic errors of the measurements of MEA and of TMB mixing ratios are cancelled out in our data analysis, since both compounds were measured by the HT-PTR-MS. The good agreement between TMB mixing ratios measured by HT-PTR-MS and GC-PID confirms the high accuracy of the TMB measurement. The overall (systematic) error of the rate constants determined in this work is composed of the error of the

27787

reference rate constant, k_{ref}, given by ±12 % (Aschmann et al., 2006) and the error of the MEA wall loss rate which translates into a ±24 % error, and is estimated to be ±27 %.

6.2 Particle formation

Amines have high particle formation potential and nucleation of particles followed by fast growth has been observed in sunlit chamber experiments with MEA (Murphy et al., 2007; Carter, 2008; Karl et al., 2010). Presence of the ionic form of dimethylamine, i.e. dimethyl aminium cation, in nucleation mode particles in boreal and marine environments led to the speculation that amines are strongly involved in post-nucleation growth (Mäkelä et al., 2001; Facchini et al., 2008). Amines may also directly participate in the first steps of nucleation, e.g. by formation of dimer clusters with sulphuric acid. Short-chained aliphatic amines like dimethylamine and trimethylamine seem to be more important than ammonia (NH$_3$) in enhancing sulphuric acid-water nucleation in the atmosphere, even though their atmospheric concentrations are usually 2–3 orders lower than that of NH$_3$ (Kurtén et al., 2008; Bzdek et al., 2010; Erupe et al., 2011). Murphy et al. (2007) observed nucleation within minutes after injection of amines in a chamber containing gaseous HNO$_3$. In this work we have assumed that new particle formation observed in MEA oxidation experiments occurs through homogenous heteromolecular nucleation between HNO$_3$ and MEA vapour molecules. Since initial HNO$_3$ mixing ratios were very low in the experiments the main source of HNO$_3$ was the reaction of photochemically produced OH with NO$_2$.

This is consistent with the observed delayed start of the nucleation burst by a few minutes after opening of the chamber canopy (Fig. 6a). Both measured and modelled number size distribution ($dN/d\log D_p$) show two separate bursts in experiment E3; the first burst after exposing the chamber to light was formed by nucleation mode particles that had formed in the dark chamber and grew by condensation of vapours, while the second burst (the nucleation burst) was formed by growing particles that nucleated short afterwards (Fig. 6a and 6b). The diameter of the growth curve (diameter of the

27788

$dN/d\log D_p$ peak) at the end of the experiment was 322 nm in the size distribution measured by SMPS and 242 nm in the size distribution obtained from the MAFOR simulation.

The observed nucleation of MEA and HNO_3 could be relevant for the atmosphere since the high numbers of particles which were produced in our experiments remained even after MEA had been largely depleted. Dissociation coefficients for aminium nitrate salts are typically one order of magnitude smaller than that of ammonium nitrate at the same temperature, with the exception of trimethylamine (Ge et al., 2011b). A recent flow tube study by Lloyd et al. (2009) demonstrated that trimethylamine can be taken up by ammonium nitrate particles, leading to an exchange of trimethylamine for NH_3 in the particles. The theoretical K_p value of ethanolaminium nitrate which was used in this work is uncertain and it was not possible to determine the true K_p value. We therefore suggest that the K_p of ethanolaminium nitrate is studied in chamber experiments with MEA and NH_3 as competing reactants for HNO_3.

The mass-based fraction of the nitrate salt in the chamber aerosol according to the AMS measurements was 23 %, 24 %, and 30 %, respectively, at the end of experiments E1, E2, and E3. The corresponding mass-based fractions of the nitrate salt predicted by MAFOR were 14 %, 20 %, and 46 % in E1, E2, and E3, respectively. Given that ethanolaminium nitrate contributed 80 % to the measured nitrate salt concentrations, the agreement is good in E1 and E2. In the case of E3 it is noted that the agreement between modelled and measured nitrate salt concentration is very good in the first two hours of the experiment (Fig. 5b). The deviation of the modelled concentration at later experiment time can be explained by the uncertainties of K_p and of the HNO_3 production rate in the model.

6.3 Application in regional modelling

The environmental impact of MEA emissions from a CO_2 capture facility due to formation and dispersion of hazardous oxidation products, photochemical ozone and particulate matter can only be realistically assessed by application of a state-of-the-

art 3-D atmospheric chemistry transport model (CTM) which includes details of the MEA chemistry. Initial work has been done by Carter (2008) who set up compressed chemistry mechanisms for several amines which have been added to the SAPRC-07 mechanism (Carter, 2010). However, these compressed mechanisms could not be evaluated in chamber experiments because of the difficulties with respect to amine quantification. The gas-phase mechanism for the OH-initiated oxidation of MEA presented in this work can be readily implemented in large scale models by using the kinetic pre-processor as for example in the WRF/Chem community model (Grell et al., 2005; http://ruc.noaa.gov/wrf/WG11/). When a CTM with a dedicated chemistry solver is used, it will be necessary to simplify the presented set of reactions. This should be done carefully in order to preserve important features of the MEA chemistry such as the NO_x-dependence of the nitramine formation.

The mass-based fraction of organics, attributed to SOA, measured by AMS was 68–76 % in experiments E1, E2, and E3. The high contribution of secondary (non-salt) organics to the aerosol formed in the OH-initiated oxidation of MEA has not been reported before and is likely a result of favourable conditions in the experiments such as sufficiently high OH-levels. The SOA formation in the presented experiments could be adequately described with a two-product approach. The non-salt organic fraction of the aerosol partly consists of relatively high-molecular organics ($>m/z$ 65), mainly C3 and C4 compounds, however individual compounds could not be identified.

An additional consideration in the mechanisms for amines is the fact that they are basic compounds that can react with atmospheric nitric acid (HNO_3) to form aminium nitrate salts, which partition into the aerosol phase. Prediction of atmospheric ozone impacts for amines will be affected by the uncertainties related to the reaction of amines with HNO_3. Modelling of the atmospheric fate of MEA is currently hampered by the highly uncertain equilibrium dissociation constant of the ethanol aminium nitrate salt, the atmospheric sources and sinks of HNO_3 and NH_3, and the presence of other amines in the atmosphere. Further, aminium salts will exist as liquid aerosols at higher humidity in the atmosphere, depending on their point of deliquescence. Once the salt

exist as a solution in water the equilibrium vapour pressure product as defined in Eq. (5) will be reduced compared to that over the solid salt, and its gas/solid dissociation constant will change as a function of RH (Ge et al., 2011b).

Despite the uncertainties in modelling of the atmospheric fate of MEA outlined above, a consequent implementation of the presented mechanisms, i.e. OH-initiated gas phase chemistry, equilibrium gas/solid partitioning of ethanolaminium nitrate and two-product SOA model, into a 3-D CTM will greatly improve environmental impact estimates.

7 Conclusions

With the help of advanced instrumentation (HT-PTR-MS and AMS) it was possible to determine the reaction rate constant relative to the rate constant of the OH + 1,3,5-trimethylbenzene reaction in EUPHORE. The chamber aerosol model MAFOR was applied to quantify losses of MEA to the particle phase. The rate constant $k(OH + MEA)$ was found to be $(9.2 \pm 1.1) \times 10^{-11}$ cm^3 molecule^{-1} s^{-1} (at 298 K) as average of two similar experiments. The reaction between OH radicals and MEA is a factor of 2–3 faster than estimated by SAR methods. Interestingly, the higher OH-reaction rate constant value found for MEA is close to rate constant values estimated by EPI Suite v4.0 for other ethanolamines. The estimated rate constants for the reaction OH and diethanolamine (DEA) and between OH and triethanolamine (TEA) are 9.3×10^{-11} cm^3 molecule^{-1} s^{-1} and 11.1×10^{-11} cm^3 molecule^{-1} s^{-1} (at 298 K), respectively.

The higher rate constant value has implications for predicted atmospheric concentrations of 2-nitroamino ethanol and formamide which are produced in the photo-oxidation of MEA. Predicted steady-state concentrations of 2-nitroamino ethanol and formamide increased by 39 % and 36 %, respectively, when applying the experimentally derived $k(OH + MEA)$ value.

Formamide, one of the major gaseous oxidation products from MEA (Nielsen et al., 2011), will be oxidized to form isocyanic acid (H−N=C=O) in the atmosphere (Barnes et al., 2010). Isocyanic acid reacts only slowly with OH and other atmospheric oxidants (Wooldridge et al., 1996) and, due to its high solubility, will be taken up in water droplets and finally be removed from the atmosphere by wet deposition. In the aqueous phase, isocyanic acid may undergo hydrolysis to form ammonia and carbon dioxide. Toxic information on isocyanic acid is sparse. Although there is no direct evidence that isocyanic acid can cause respiratory sensitisation, it is a biologically reactive compound and can cause damage to biological systems (Shah et al., 2008). Exposure to elevated levels (>1 ppbv) of isocyanic acid and its dissociated form, the cyanate ion (NCO$^-$), have been related to atherosclerosis, cataracts, and rheumatoid arthritis in humans (Roberts et al., 2011).

Nitramines may have carcinogenic effects and, in contrary to nitrosamines, are photochemically stable in the atmosphere (Grosjean, 1991) and can have atmospheric lifetimes of more than 2 days. Using atmospheric average 12-h daytime OH concentrations of 1.5×10^6 radicals cm^{-3} and the reported rate constant for the reaction with OH radicals (Tuazon et al., 1984), updated with the recommended value for the reference rate of CH$_3$OCH$_3$ ($k(OH + CH_3OCH_3) = 2.8 \times 10^{-12}$ cm^3 molecule^{-1} s^{-1} at 298 K; IUPAC, 2009), the atmospheric lifetime of dimethylnitramine is estimated to be 2.41 days. Using the estimated rate constant of OH radicals with 2-nitroamino ethanol obtained by EPI Suite version 4.0, indicates a shorter lifetime for this nitramine, i.e. 0.52 days. Due to the expected long lifetimes towards reaction with OH radicals, further studies on the toxicity of nitramines, which form in the atmospheric degradation of amines, are recommended.

Appendix A

Relative rate equation

Integration of the balances equations in Eq. (9) from $t' = 0$ to $t' = t$ gives the following set of equations:

$$\ln\left(\frac{<\text{MEA}(0)>}{<\text{MEA}(t)>}\right) = k_1 \int_0^t [\text{OH}]dt' + \int_0^t k_{\text{dil}}(t')dt' + \int_0^t \left(k_{\text{wall}}(t') + k_{\text{particles}}(t')\right)dt' \tag{A1}$$

$$\ln\left(\frac{<\text{TMB}(0)>}{<\text{TMB}(t)>}\right) = k_{\text{ref}} \int_0^t [\text{OH}]dt' + \int_0^t k_{\text{dil}}(t')dt' \tag{A2}$$

$$\ln\left(\frac{<\text{SF}_6(0)>}{<\text{SF}_6(t)>}\right) = \int_0^t k_{\text{dil}}(t')dt' \tag{A3}$$

For the analyzed time period of the experiment, temperature was almost constant and it is thus assumed that the OH rate constants k_1 and k_{ref} do not vary over time. Introducing short-cuts for the logarithmic relative concentrations,

$$Y_{\text{MEA}}(t) = \ln\left(\frac{<\text{MEA}(0)>}{<\text{MEA}(t)>}\right) \tag{A4}$$

$$X_{\text{TMB}}(t) = \ln\left(\frac{<\text{TMB}(0)>}{<\text{TMB}(t)>}\right) \tag{A5}$$

$$D_{\text{SF}_6}(t) = \ln\left(\frac{<\text{SF}_6(0)>}{<\text{SF}_6(t)>}\right) \tag{A6}$$

and an integrated loss rate,

27793

$$L(t) = \int_0^t \left(k_{\text{wall}}(t') + k_{\text{particles}}(t')\right)dt' \tag{A7}$$

results in a modified relative rate equation:

$$Y_{\text{MEA}}(t) - D_{\text{SF}_6}(t) - L(t) = \frac{k_1}{k_{\text{ref}}}\left(X_{\text{TMB}}(t) - D_{\text{SF}_6}(t)\right) \tag{A8}$$

This expression can be further simplified by introducing new variables which can be calculated based on measured time series:

$$Y'_{\text{MEA}}(t) = Y_{\text{MEA}}(t) - D_{\text{SF}_6}(t) - L(t) \tag{A9}$$

$$X'_{\text{TMB}}(t) = X_{\text{TMB}}(t) - D_{\text{SF}_6}(t) \tag{A10}$$

By replacing the terms in Eq. (A8) with Y'_{MEA} and X'_{TMB} as given in Eq. (A9) and Eq. (A10), a standard relative rate equation is derived.

27794

References

Angelino, S., Suess, D. T., and Prather, K. A.: Formation of aerosol particles from reactions of secondary and tertiary alkylamines: Characterization by aerosol time-of-flight mass spectrometry, Environ. Sci. Technol., 40, 3130–3138, 2001. 27766

Aschmann, S. M., Long, W. D., and Atkinson, R.: Temperature-dependent rate constants for the gas-phase reactions of OH radicals with 1,3,5-trimethylbenzene, triethyl phosphate, and a series of alkylphosphonates. J. Phys. Chem. A, 110, 7393–7400, 2006. 27782, 27787, 27788, 27804, 27808

Bakovic, M., Fullerton, M. D., and Michel, V.: Metabolic and molecular aspects of ethanolamine phospholipid biosynthesis: the role of CTP: phosphoethanolamine cytidylyltransferase (Pcyt2). Biochem. Cell Biol., 85, 283–300, 2007. 27765

Barnes, I., Solignac, G., Mellouki, A., and Becker, K. H.: Aspects of the atmospheric chemistry of amides, Chem. Phys. Chem., 11, 3844–3857, 2010. 27775, 27792, 27805

Becker, K. H.: The European photoreactor EUPHORE. Final report of the EC-Project contract EV5V-CT02-0059, Physikalische Chemie, Bergische Universität-Gesamthochschule Wuppertal, Wuppertal, Germany, 1996. 27767

Bilde, M., Svenningsson, B., Monster, J., and Rosenørn, T.: Even-odd alternation of evaporation rates and vapor pressures of C3-C9 dicarboxylic acid aerosols, Environ. Sci. Technol., 37, 1371–1378, 2003. 27806

Bloss, C., Wagner, V., Bonzanini, A., Jenkin, M. E., Wirtz, K., Martin-Reviejo, M., and Pilling, M. J.: Evaluation of detailed aromatic mechanisms (MCMv3 and MCMv3.1) against environmental chamber data, Atmos. Chem. Phys., 5, 623–639, doi:10.5194/acp-5-623-2005, 2005a. 27775

Bloss, C., Wagner, V., Jenkin, M. E., Volkamer, R., Bloss, W. J., Lee, J. D., Heard, D. E., Wirtz, K., Martin-Reviejo, M., Rea, G., Wenger, J. C., and Pilling, M. J.: Development of a detailed chemical mechanism (MCMv3.1) for the atmospheric oxidation of aromatic hydrocarbons, Atmos. Chem. Phys., 5, 641–664, doi:10.5194/acp-5-641-2005, 2005b. 27804, 27805

Brauers, T. and Finlayson-Pitts, B. J.: Analysis of relative rate measurements, Int. J. Chem. Kinet., 29, 665–672, 1997. 27783

Bråten, H. B., Bunkan, A. J., Bache-Andreassen, L., Solimannejad, M., and Nielsen, C. J.: Final report on a theoretical study on the atmospheric degradation of selected amines, NILU OR 77/2008, Norwegian Institute for Air Research, Kjeller, Norway, available at http://www.nilu.

27795

no, 2008. 27775

Bzdek, B. R., Ridge, D. P., and Johnston, M. V.: Amine exchange into ammonium bisulfate and ammonium nitrate nuclei, Atmos. Chem. Phys., 10, 3495–3503, doi:10.5194/acp-10-3495-2010, 2010. 27788

Carter, W. P. L.: Reactivity estimates for selected consumer product compounds, Final Report, Contract No. 06-408, Center for Environmental Research and Technology, College of Engineering, University of California, Riverside, California, USA, available at http://www.engr.ucr.edu/~carter/pubs/aminrep.pdf, 2008. 27766, 27788, 27790, 27808

Carter, W. P. L.: Development of the SAPRC-07 chemical mechanism and updated ozone reactivity scales, Report to the California Air Resources Board, Contracts No. 03-318, 06-408, and 07-730, Riverside CA, USA, available at: http://www.cert.ucr.edu/~carter/SAPRC/saprc07.pdf, 2010. 27766, 27790, 27804

Cocker, D. R., Mader, B. T., Kalberer, M., Flagan, R. C., and Seinfeld, J. H.: The effect of water on gas-particle partitioning of secondary organic aerosol: II. m-xylene and 1,3,5-trimethylbenzene photooxidation systems, Atmos. Environ., 35, 6073–6085, 2001. 27778

DiGuilio, R. M., Lee, R. J., Schaeffer, S. T., Brasher, L. L., and Teja, A. S.: Densities and viscosities of the ethanolamines, J. Chem. Eng. Data, 37, 239–242, 1992. 27764

Dow Chemicals, available at: http://www.dow.com/amines/prod/ethano-mea.htm, 2011. 27764

Drewnick, F., Hings, S. S., DeCarlo, P. F., Jayne, J. T., Gonin, M., Fuhrer, K., Weimer, S., Jimenez, J. L., Demerjian, K. L., Borrmann, S., and Worsnop, D. R.: A new Time-of-Flight Aerosol Mass Spectrometer (ToF-AMS) – Instrument Description and First Field Deployment, Aerosol Sci. Technol., 39, 637–658, 2005. 27771

Erupe, M. E., Viggiano, A. A., and Lee, S.-H.: The effect of trimethylamine on atmospheric nucleation involving H_2SO_4, Atmos. Chem. Phys., 11, 4767–4775, doi:10.5194/acp-11-4767-2011, 2011. 27788

Facchini, M. C., Decesari, S., Rinaldi, M., Carbone, C., Finessi, E., Mircea, M., Fuzzi, S., Moretti, F., Tagliavini, E., Ceburnis, D., and O'Dowd, C. D.: Important source of marine secondary organic aerosol from biogenic amines. Environ. Sci. Technol., 42, 9116–9121, 2008. 27788

Fahlman, A.: A modified Marquardt-Levenberg parameter estimation routine for Matlab, Report NMRC 01-002, Naval Medical Research Institute, Bethesda, MD, USA, 2001. 27777, 27806

Fournier, M., Lesage, J., Ostiguy, C., and Tra, H. V.: Sampling and analytical methodology development for the determination of primary and secondary low molecular weight amines

27796

in ambient air, J. Environ. Monit., 10, 379–386, 2008. 27772

Fuchs, N. A. and Sutugin, A. G.: Highly Dispersed Aerosols, Ann. Arbor Sci., Ann Arbor, Mich., USA, 1970. 27779

Ge, X., Wexler, A. S., and Clegg, S. L.: Atmospheric amines – Part I: A review, Atmos. Environ., 45, 524–546, 2011a. 27765

Ge, X., Wexler, A. S., and Clegg, S. L.: Atmospheric amines - Part II: Thermodynamic properties and gas/particle partitioning, Atmos. Environ., 45, 561–577, 2011b. 27779, 27789, 27791

Geier, J., Lessmann, H., Dickel, H., Frosch, P. J., Koch, P., Becker, D., Jappe, U., Aberer, W., Schnuch, A., Uter, W.: Patch test results with the metalworking fluid series of the German Contact Dermatitis Research Group (DKG), Contact Dermatitis, 51, 118–130, 2004. 27764

Geiger, H., Barnes, I. Becker, K. H., Bohn, B., Brauers, T., Donner, B., Dorn, H.-P., Elend, M., Freitas Dinis, C. M., Grossmann, D., Hass, H., Hein, H., Hoffmann, A., Hoppe, L., Hülsemann, F., Kley, D., Klotz, B., Libuda, H. G., Maurer, T., Mihelcic, D., Moortgat, G. K., Olariu, R., Neeb, P., Poppe, D., Ruppert, L., Sauer, C. G., Shestakov, O., Somnitz, H., Stockwell, W. R., Thüner, L. P., Wahner, A., Wiesen, P., Zabel, F., Zellner, R., Zetzsch, C.: Chemical mechanism development: Laboratory study and model applications, J. Atmos. Chem., 42, 323–357, 2002. 27787

Goff, G. S. and Rochelle, G. T.: Monoethanolamine degradation: O_2 mass transfer effects under CO_2 capture conditions, Ind. Eng. Chem. Res., 43, 6400–6408, 2004. 27765

Goodall, C. M. and Kennedy, T. H.: Carcinogenicity of dimethylnitramine in NZR rats and NZO mice, Cancer Lett., 1, 295–298, 1976. 27766

Güsten, H.: Predicting the abiotic degradability of organic pollutants in the troposphere. Chemosphere, 38, 1361–1370, 199. 27776

Grell, G. A., Peckham, S. E., Schmitz, R., McKeen, S. A., Frost, G., Skamarock, W. C., and Eder, B.: Fully coupled online chemistry within the WRF model, Atmos. Environ., 39, 6957–6975, 2005. 27790

Grosjean, D.: Atmospheric chemistry of toxic contaminants: 6. Nitrosamines: Dialkyl nitrosamines and nitrosomorpholine, J. Air Waste Manage. Assoc., 41, 306–311, 1991. 27765, 27792

Hassel, M., Frei, E., Streeter, A. J., and Wiessler, M.: Pharmakokinetics of N-nitrodimethylamine and N-nitromethylamine in the rat, Carcinogenesis, 11, 357–360, 1990. 27766

27797

IUPAC Subcommittee for Gas Kinetic Data Evaluation 2009, Evaluated kinetic data, http://www.iupac-kinetic.ch.cam.ac.uk/index.html, 2009. 27792

Jacobson, M. Z.: Numerical techniques to solve condensational and dissolutional growth equations when growth is coupled to reversible reactions, Aerosol Sci. Technol., 27, 491–498, 1997. 27773, 27804

Jacobson, M. Z.: Effects of ethanol (E85) versus gasoline vehicles on cancer and mortality in the United States, Environ. Sci. Technol., 41, 4150–4157, 2007. 27804

Jordan, A., Haidacher, S., Hanel, G., Hartungen, E., Märk, L., Seehauser, H., Schottkowsky, H., Sulzer, P., Märk, T. D.: A high resolution and high sensitivity proton-transfer-reaction time-of-flight mass spectrometer (PTR-TOF-MS), Int. J. Mass Spectrom., 286(2–3), 122–128, 2009. 27770

Kapteina, S., Slowik, K., Verevkin, S. P., and Heintz, A.: Vapor pressures and vaporization enthalpies of a series of ethanolamines. J. Chem. Eng. Data, 50, 398–402, 2005. 27765

Karl, M., Gross, A., Leck, C., and Pirjola, L.: Intercomparison of dimethylsulfide oxidation mechanisms for the marine boundary layer: Gaseous and particulate sulfur constituents, J. Geophys. Res., 112, D15304, doi:10.1029/2006JD007914, 2007. 27774

Karl, M., D'Anna, B., George, C., King, S., Wisthaler, A., Dye, C., and Nielsen, C. J.: Particle formation in photo-oxidation experiments with 2-aminoethanol (MEA), Geophys. Res. Abs., 12, EGU2010-8196, 2010. 27788

Karl, M., Wright, R. F., Berglen, T. F., and Denby, B.: Worst case scenario study to assess the environmental impact of amine emissions from a CO_2 capture plant, Int. J. Greenhouse Gas Control, 5, 439–447, 2011a. 27766

Karl, M., Gross, A., Leck, C., and Pirjola, L.: A new flexible multicomponent model for the study of aerosol dynamics in the marine boundary layer, Tellus B, doi:10.1111/j.1600-0889.2011.00562.x, available online, 2011b. 27773

Koornneef, J., van Keulen, T., Faaij, A., and Turkenburg, W.: Life cycle assessment of a pulverized coal power plant with post-combustion capture, transport and storage of CO_2, Int. J. Greenhouse Gas Control, 2, 448–467, 2008. 27765

Kurtén, T., Loukonen, V., Vehkamäki, H., and Kulmala, M.: Amines are likely to enhance neutral and ion-induced sulfuric acid-water nucleation in the atmosphere more effectively than ammonia, Atmos. Chem. Phys., 8, 4095–4103, doi:10.5194/acp-8-4095-2008, 2008. 27788

Kwok, E. S. C. and Atkinson, R.: Estimation of hydroxyl radical reaction rate constants for gas-phase organic compounds using a structure-reactivity relationship: An update. Atmos.

27798

Environ., 29, 1685–1695, 1995. 27766, 27776

Landgraf, J. and Crutzen, P. J.: An efficient method for online calculations of photolysis and heating rates, J. Atmos. Sci., 55, 863–878, 1998. 27774

Lepaumier, H., Picq, D., and Carrette, P. L.: Degradation study of new solvents for CO_2 capture in post-combustion, Greenhouse Gas Control Technologies 9, Proceedings of the 9th International Conference on Greenhouse Gas Control Technologies (GHGT-9), 16–20 November 2008, Washington DC, USA, Energy Procedia, 1, 893–900, 2009. 27764

Lloyd, J. A., Heaton, K. J., and Johnston, M. V.: Reactive uptake of trimethylamine into ammonium nitrate particles, J. Phys. Chem. A, 113, 4840–4843, 2009. 27789

Mäkelä, J. M., Yli-Koivisto, S., Hiltunen, V., Seidl, W., Swietlicki, E., Teinila, K., Sillanpaa, M., Koponen, I. K., Paatero, J., Rosman, K., and Hameri, K.: Chemical composition of aerosol during particle formation events in boreal forest, Tellus B, 53, 380–393, 2001. 27788

Meylan, W. and Howard, P. H.: User's Guide for APOWIN, Version 1.9. Syracuse Research Corporation, North Syracuse (NY), USA, 2000. 27776

Meylan, W. M. and Howard, P. H.: A review of quantitative structure-activity relationship methods for the prediction of atmospheric oxidation of organic chemicals. Environ. Toxicol. Chem., 22, 1724–1732, 2003. 27766, 27776

Mikoviny, T., Kaser, L., and Wisthaler, A.: Development and characterization of a High-Temperature Proton-Transfer-Reaction Mass Spectrometer (HT-PTR-MS), Atmos. Meas. Tech., 3, 537–544, doi:10.5194/amt-3-537-2010, 2010. 27769

Mirvish, S. S., Bulay, O., Runge, R. G., and Patil, K.: Study of the carcinogenicity of large doses of dimethylnitramine, N-nitroso-1-proline and sodium nitrite administered in drinking water to rats, J. Natl. Cancer Inst., 64, 1435–1439, 1980. 27766

Müller, M., George, C., and D'Anna, B.: Enhanced spectral analysis of C-TOF Aerosol Mass Spectrometer data: Iterative residual analysis and cumulative peak fitting, Int. J. Mass Spectrom., 306, 1–8, 2011. 27771

Murphy, S. M., Sorooshian, A., Kroll, J. H., Ng, N. L., Chhabra, P., Tong, C., Surratt, J. D., Knipping, E., Flagan, R. C., and Seinfeld, J. H.: Secondary aerosol formation from atmospheric reactions of aliphatic amines, Atmos. Chem. Phys., 7, 2313–2337, doi:10.5194/acp-7-2313-2007, 2007. 27766, 27767, 27788

Naumann, K. H.: COSIMA – a computer program simulating the dynamics of fractal aerosols, J. Aerosol Sci., 34, 1371–1397, 2003. 27775

Nielsen, C. J., D'Anna, B., Dye, C., George, C., Graus, M., Hansel, A., Karl, M., King, S.,

Musabila, M., Müller, M., Schmidbauer, N., Stenstrøm, Y., and Wisthaler, A.: Atmospheric Degradation of Amines, Summary Report: Gas phase oxidation of 2-aminoethanol (MEA), CLIMIT project no. 193438, NILU OR 8/2010, Norwegian Institute for Air Research, Kjeller, Norway, available at: http://www.nilu.no, 2010. 27766, 27769, 27771, 27775, 27776, 27780, 27805

Nielsen, C. J., D'Anna, B., Dye, C., Graus, M., Karl, M., King, S., Musabila, M., Müller, M., Schmidbauer, N., Stenstrøm, Y., Wisthaler, A., and Pedersen, S.: Atmospheric chemistry of 2-aminoethanol (MEA), Energy Procedia, 4, 2245–2252, 2011. 27765, 27766, 27775, 27776, 27785, 27792

NVE, Carbon Capture and Storage at Kårstø, Svendsen P. T. (Ed.), Norwegian Water Resources and Energy Directorate, available at: http://www.nve.no, 2006. 27765

Odum, J. R., Hoffmann, T., Bowman, F., Collins, D., Flagan, R. C., and Seinfeld, J. H.: Gas/particle partitioning and secondary organic aerosol yields, Environ. Sci. Technol., 30, 2580–2585, 1996. 27776, 27806

Odum, J. R., Jungkamp, P. W., Griffin, R. J., Flagan, R. C., and Seinfeld, J. H.: The atmospheric aerosol-forming potential of whole gasoline vapor, Science, 276, 96–99, 1997. 27776

Papa, E. and Gramatica, P.: Externally validated QSPR modeling of VOC tropospheric oxidation by NO_3 radicals, SAR and QSAR in Environmental Research, 19, 655–668, 2008. 27786

Pitts, J. N., Grosjean, D., Vanmcauwenberghe, K., Schmidt, J. P. and Fitz, D. R.: Photooxidation of aliphatic amines under simulated atmospheric conditions: Formation of nitrosamines, nitramines, amides, and photochemical oxidant, Environ. Sci. Technol., 12, 946–953, 1978. 27765

Press, W. H., Teukolsky, S. A., Vetterling, W. T., and Flanenry, B. P., *Numerical Recipes in C*, Cambridge University Press, Cambridge, United Kingdom, Chap. 15, 1992. 27783

Puxty, G., Rowland, R., Allport, A., Yang, Q., Bown, M., Burns, R., Maeder, M., and Attalla, M.: Carbon dioxide post-combustion capture: a novel screening study of the carbon dioxide absorption performance of 76 amines. Environ. Sci. Technol., 43, 6427–6433, 2009. 27764

Rao, A. B. and Rubin, E. S.: A technical, economic, and environmental assessment of amine-based CO_2 capture technology for power plant greenhouse gas control, Environ. Sci. Technol., 36, 4467–4475, 2002. 27765

Roberts, J. M., Veres, P. R., Cochran, A. K., Warneke, C., Burling, I. R., Yokelson, R. J., Lerner, B., Gilman, J. B., Kuster, W. C., Fall, R., and de Gouw, J.: Isocyanic acid in the atmosphere and its possible link to smoke-related health effects, P. Natl. Acad. Sci., 108, 8966–8971,

2011. 27792

Rochelle, G. T.: Amine scrubbing for CO_2 capture, Science, 325, 1652–1653, 2009. 27764

Ródenas, M.: Improvements in spectroscopy data processing: faster production and better reliability of Lab data, INTROP Report, available at:: http://www.ceam.es/pag/contam_e_archivos/MRodenasINTROPReport.pdf, 2008. 27770

Sander, R., Kerkweg, A., Jöckel, P., and Lelieveld, J.: Technical note: The new comprehensive atmospheric chemistry module MECCA, Atmos. Chem. Phys., 5, 445–450, doi:10.5194/acp-5-445-2005, 2005. 27774

Sander, R., Baumgaertner, A., Gromov, S., Harder, H., Jöckel, P., Kerkweg, A., Kubistin, D., Regelin, E., Riede, H., Sandu, A., Taraborrelli, D., Tost, H., and Xie, Z.-Q.: The atmospheric chemistry box model CAABA/MECCA-3.0, Geosci. Model Dev., 4, 373–380, doi:10.5194/gmd-4-373-2011, 2011. 27774

Sander, S. P., Friedl, R. R., Golden, D. M., Kurylo, M. J., Moortgat, G. K., Keller-Rudek, H., Wine, P. H., Ravishankara, A. R., Kolb, C. E., Molina, M. J., Finlayson-Pitts, B. J., Huie, R. E., and Orkin, V. L.: Chemical Kinetics and Photochemical Data for Use in Atmospheric Studies, Evaluation Number 15, JPL Publication 06-2, Jet Propulsion Laboratory, Pasadena, CA, 2006. 27774

Sandu, A. and Sander, R.: Technical note: Simulating chemical systems in Fortran90 and Matlab with the Kinetic PreProcessor KPP-2.1, Atmos. Chem. Phys., 6, 187–195, doi:10.5194/acp-6-187-2006, 2006. 27774

Sandu, A., Verwer, J. G., Van Loon, M., Carmichael, G. R., Potra, F. A., Dabdub, D., and Seinfeld, J. H.: Benchmarking stiff ODE solvers for atmospheric, chemistry problems .1. Implicit vs explicit, Atmos. Environ., 31, 3151–3166, 1997. 27774

Scherf, H. R., Frei, E., and Wiessler, M.: Carcinogenic properties of N-nitrodimethylamine and N-nitromethylamine in the rat, Carcinogenesis, 10, 1977–1981, 1989. 27766

Seinfeld, J. H. and Pandis, S. N., *Atmospheric Chemistry and Physics: From Air Pollution to Climate Change*, Chapter 9.4: Thermodynamics of Atmospheric Aerosol Systems, 534 pp., Wiley, New York, USA, 1998. 27779

Seinfeld, J. H. and Pankow, J. F.: Organic atmospheric particulate material, Annu. Rev. Phys. Chem., 54, 121–140, 2003. 27777

Shah S. V., Apostolov, E. O., Ok, E., and Basnakian, A. G.: Novel mechanisms in accelerated atherosclerosis in kidney disease, J. Ren. Nut., 18, 65–69, 2008. 27792

Smith, J. N., Barsanti, K. C., Friedli, H. R., Ehn, M., Kulmala, M., Collins, D. R., Scheckman,

J. H., Williams, B. J., and McMurry, P. H.: Observations of aminium salts in atmospheric nanoparticles and possible climatic implications, P. Natl. Acad. Sci., 107, 66434–66439, 2010. 27766

Sorooshian, A., Murphy, S. M., Hersey, S., Gates, H., Padro, L. T., Nenes, A., Brechtel, F. J., Jonsson, H., Flagan, R. C., and Seinfeld, J. H.: Comprehensive airborne characterization of aerosol from a major bovine source, Atmos. Chem. Phys., 8, 5489–5520, doi:10.5194/acp-8-5489-2008, 2008. 27766

Suzuki, E., Mochizuki, M., Sekiguchi, N., Osabe, M., and Okada, M.: In vitro metabolism of N-nitrodialkylamines, Jpn. J. Cancer Res., 76, 28–36, 1985. 27766

Thitakamol, B., Veawab, A., and Aroonwilas, A.: Environmental impacts of absorption-based CO_2 capture unit for post-combustion treatment of flue gas from coal-fired power plant, Int. J. Greenhouse Gas Control, 1, 318–342, 2007. 27765

Todeschini, R., Consonni, V., Mauri, A., and Pavan, M.: DRAGON version 6, Talete srl, Milan, Italy, available online at http://www.talete.mi.it/, 2011. 27787

Tuazon, E. C., Carter, W. P. L., Atkinson, R., Winer, A. M., and Pitts, J. N., Jr.: Atmospheric reactions of N-nitrosodimethylamine and dimethylnitramine, Environ. Sci. Technol., 18, 49–54, 1984. 27792

U.S. EPA, Estimation Programs Interface Suite™ for Microsoft Windows, v 4.00, United States Environmental Protection Agency, Washington, DC, Office of Pollution Prevention and Toxics, Syracuse (NY): Syracuse Research Corporation, available at: http://www.epa.gov/oppt/exposure/pubs/episuite.htm, 2009. 27776

Veltman, K., Singh, B., and Hertwich, E. G.: Human and environmental impact assessment of postcombustion CO_2 capture focusing on emissions from amine-based scrubbing solvents to air, Environ. Sci. Technol., 44, 1496–1502, doi:10.1021/es902116r, 2010. 27765

Vera, T., Muñoz, A., Ródenas, M., Vázquez, M., Borrás, E., Marqués, M., Mellouki, A., Treacy, J., and Sidebottom, H.: Atmospheric fate of hymexazol (5-methylisoxazol-3-ol): Simulation chamber studies, Atmos. Environ., 45, 3704–3710, 2011. 27767

Wooldridge, S. T., Hanson, R. K., and Bowman, C. T.: A shock tube study of reactions of CN with HCN, OH, and H_2 using CN and OH laser absorption, Int. J. Chem. Kinet., 28, 245–258, 1996. 27792

Zádor, J., Turányi, T., Wirtz, K., and Pilling, M. J.: Measurement and investigation of chamber radical sources in the European Photoreactor (EUPHORE), J. Atmos. Chem., 55, 147–166, 2006. 27774

Table 1. Range of the mixing ratios of O_3, NO, NO_2, average relative humidity and average temperature in the MEA photo-oxidation experiments.

Exp.	Date	O_3 (ppbv)	NO_2 (ppbv)	NO (ppbv)	RH (%)	T (K)
E1	28.07.2010	0–80	5–55	0–30	7 ± 1	304.9 ± 2.0
E2	28.07.2010	0–120	5–70	2	10 ± 1	307.4 ± 1.6
E3	27.07.2010	10–25	140–225	20–140	11 ± 6	306.9 ± 0.1
E4	15.05.2009	0–70	0–20	0–30	2 ± 1	300.3 ± 1.3
E5	11.05.2009	<1	340–460	690–740	3 ± 1	299.5 ± 1.8

Table 2. Simplified reaction mechanism for 1,3,5-trimethylbenzene used in this study. The degree of detail of this mechanism corresponds to the aromatic hydrocarbon chemistry scheme by Jacobson (1997).

No.	Reaction			Rate constant[a]	Reference
1	TMB + OH	→	0.79 TMBADO2 + 0.21 AROPEN + 0.03 TMBO2 + 0.05 CRES + 0.05 HO_2 + 0.04 TMBSOA	$4.40 \times 10^{-12} \exp(738/T)$	Aschmann et al. (2006)
2	TMBO2 + NO	→	0.105 TMBNIT + 0.895 TMBO + 0.895 NO_2	$2.54 \times 10^{-12} \exp(360/T)$	MCM[b]
3	TMBO + O_2	→	1.28 CRES + 1.28 HO_2	9.5×10^{-15}	MCM[b]
4	TMBADO2+O_2	→	0.157 TMBNIT + 0.843 TMBADO + 0.843 NO_2	$2.54 \times 10^{-12} \exp(360/T)$	MCM[b]
5	TMBADO2	→	1.2 TMBADO + 0.51 CRES + 0.51 BZALD + 1.2 MGLYOX	$2.4 \times 10^{-12} \times [RO_2]$	MCM[b]
6	TMBADO	→	MGLYOX + HO_2 + 0.5 AROPEN + 0.5 DCB1	1.0×10^{6}	MCM[b]
7	AROPEN + OH	→	AROPPX + CH_3CO_3 + HO_2 + CO	3.0×10^{-11}	Jacobson (2007)
8	AROPPX + NO	→	NO_2 + HCHO + HO_2 + CO	8.1×10^{-12}	Jacobson (2007)
9	CRES + OH	→	0.24 BZO + 0.76 CRESO2 + H_2O	$1.7 \times 10^{-12} \exp(950/T)$	Carter (2010)
10	CRESO2 + NO	→	0.58 AROPEN + 0.58 ARACID + NO_2 + HO_2	4.0×10^{-12}	Jacobson (2007)
11	BZO + NO_2	→	BZN	$2.3 \times 10^{-12} \exp(150/T)$	Carter (2010)
12	AROPEN + $h\nu$	→	$CH_3C(O)OO$ + CO + HO_2	j(MGLYOX)	MCM[c]
13	BZALD + $h\nu$	→	PHO2 + CO + HO_2	j(MGLYOX)	MCM[c]

[a] Rate constant in units cm^3 molecule^{-1} s^{-1}, photolysis rates in units s^{-1}.

[b] Rate constant and branching ratio adopted from the Master Chemical Mechanism (MCM) v3.1 (Bloss et al., 2005b), available at http://mcm.leeds.ac.uk/MCMv3.1.

[c] Photolysis rate parameterization as J(34) in MCM v3.1.

Table 3. Mechanism for OH-initiated oxidation of MEA used to simulate chamber experiments on the photo-oxidation of MEA[a]. Reactions with gas-phase products and temperature dependent rate constants.

No.	Reaction		Rate constant[b]	Reference
1	$NH_2CH_2CH_2OH + OH$	$\rightarrow$ 0.05 H_2NCH_2CHO + 0.8 MEABO2 + 0.15 MEAN + 0.05 HO_2	3.58×10^{-11}	EPI Suite™v4.0
2	$H_2NCH_2CHO + OH$	$\rightarrow$ 0.8 $H_2NCH_2CO_3$ + 0.2 H_2NCHO_2CHO + H_2O	4.83×10^{-11}	EPI Suite™ v4.0
3	$H_2NCH_2O_3 + NO$	$\rightarrow$ MMAO2 + CO_2 + NO_2	8.10×10^{-12} exp(270/T)	MCM[c]
4	$H_2NCHO_2CHO + NO$	$\rightarrow$ $H_2NCOCHO$ + HO_2 + NO_2	1.7×10^{-11}	This work, estimate
5	$H_2NCOCHO + OH$	$\rightarrow$ H_2NCOCO_3 + H_2O	1.47×10^{-11}	EPI Suite™ v4.0
6	$H_2NCOCO_3 + NO$	$\rightarrow$ H_2NCHO + CO_2 + NO_2	8.10×10^{-12} exp(270/T)	MCM[c]
7	MEABO2 + NO	$\rightarrow$ MEABO + NO_2	2.54×10^{-12} exp(360/T)	MCM[c]
8	MEABO + O_2	$\rightarrow$ H_2NCOCH_2OH + HO_2	2.4×10^{-15}	This work, estimate
9	MEABO	$\rightarrow$ H_2NCHO + HCHO	2.0×10^{5}	This work, estimate
10	$H_2NCHO + OH$	$\rightarrow$ HNCO + HO_2	4.0×10^{-12}	Barnes et al. (2010)
11	$H_2NCOCH_2OH + OH$	$\rightarrow$ $H_2NCOCHO$ + HO_2	4.59×10^{-12}	EPI Suite™ v4.0
12	MEAN + NO_2	$\rightarrow$ 0.5 MEANNO2 + 0.5 $HNCHCH_2OH$ + 0.5 HONO	1.4×10^{-13}	Nielsen et al. (2010)[d]
13	MEAN + O_2	$\rightarrow$ $HNCHCH_2OH$ + HO_2	1.2×10^{-19}	Nielsen et al. (2010)[d]
14	MEAN + NO	$\rightarrow$ MEANNO	8.5×10^{-14}	Nielsen et al. (2010)[d]
15	MEANNO2 + OH	$\rightarrow$ MEANHA + HO_2	1.48×10^{-11}	EPI Suite™ v4.0

[a] List of model surrogate compounds and compounds with shortname: MEAN: N-amino ethanol radical, MEABO2: C2-amine peroxy radical, MEABO: C2-amine alkoxy radical, MEANNO: 2-(N-nitrosoamino)-ethanol, MEANNO2: 2-nitroamino ethanol, MEANHA: N-nitro hydroxyacetamide, MMAO2: methylamine peroxy radical.

[b] Rate constant in units cm^3 molecule^{-1} s^{-1} for bimolecular reactions.

[c] Generic rate constant adopted from the Master Chemical Mechanism (MCM) v3.1 (Bloss et al., 2005b), available at http://mcm.leeds.ac.uk/MCMv3.1.

[d] Rate constant estimated based on analogous dimethylamine reactions.

Table 4. Parameters of the two product partitioning approach for SOA[a] formed in reaction OH + MEA.

SOA product	α (mass-based[b])	p_L^0 (Pa at 296 K)	ΔH_{vap} (kJmol^{-1})	MW (gmol^{-1})
MEAp1	0.76 ± 0.04	3.9×10^{-5c}	138[c]	126
MEAp2	0.09 ± 0.01	3.9×10^{-7d}	138[d]	126

[a] The SOA yield Y^{SOA} can be expressed as a function of ΔM_o by (Odum et al., 1996):

$$Y^{SOA} = \Delta M_o \sum_i \frac{\alpha_i K_{om,i}}{1 + K_{om,i} \Delta M_o}$$

where $K_{om,i}$ of a SOA compound i is defined as $K_{om,i} = K_{p,i}^{SOA}/f$, with and f being the absorptive mass fraction. The gas phase/particle partitioning coefficient, $K_{p,i}^{SOA}$, is calculated according to:

$$K_{p,i}^{SOA} = \frac{10^{-6} RTf}{MW \zeta_i p_{L,i}^0}$$

where the activity coefficient ζ_i is unity, and R is the universal gas constant (8.206×10^{-5} m^3 atm mol^{-1} K^{-1}).

[b] Mass-based stoichiometric yields α_1 and α_2 were determined from fit to experimental data assuming a two-product model using a modified Marquardt-Levenberg parameter estimation method (Fahlman, 2001). Given errors are statistical errors of the measurements of M_o and MEA. Fitting the experimental data with a one-product model resulted $\alpha_1 = 0.80 \pm 0.04$.

[c] Vapour pressure (p_L^0) and enthalpy of vaporization (ΔH_{vap}) of succinic acid, adopted from Bilde et al. (2003).

[d] Vapour pressure of MEAp2 is a factor of 100 lower than that of MEAp1.

Table 5. Loss rates in Experiment E1 and E2. Particle loss given as model average particle loss rate (according to Eq. 3) in the first half hour of the sunlit experiment.

Experiment	k_{dil} [a] (s^{-1})	k_{wall} [a] (s^{-1})	$k_{particles}$ [b] (s^{-1})
E1	$(2.45 \pm 0.74) \times 10^{-5}$	$(1.86 \pm 0.65) \times 10^{-4}$	$(7.0 \pm 2.7) \times 10^{-6}$
E2	$(3.12 \pm 0.34) \times 10^{-5}$	$(2.32 \pm 0.86) \times 10^{-4}$	$(4.8 \pm 0.5) \times 10^{-6}$

[a] 1-σ variance from least square fit weighted by measurement uncertainties.
[b] Standard deviation of the average modelled particle loss rate.

Table 6. Rate constant $k(OH + MEA)$ values estimated by SAR and as determined in Experiment E1 and E2. LSQ parameters and their uncertainties are provided for the experimentally derived rate constant values.

Method	$k(OH + MEA)$ (cm^3 molecule^{-1} s^{-1})	Temp. (K)	LSQ parameters a	b [a]	Reference
SAR Estimate	3.58×10^{-11}	298.25			EPI Suite™ v4.0
SAR Estimate	4.41×10^{-11}	300.0			Carter (2008)
E1, LSQ	$(9.3 \pm 1.0) \times 10^{-11}$	303.6 ± 0.4	-0.04 ± 0.01	1.86 ± 0.08	This work
E2, LSQ	$(8.1 \pm 0.8) \times 10^{-11}$	306.6 ± 1.4	-0.03 ± 0.02	1.65 ± 0.07	This work

[a] it is $b = k/k_{ref}$, where k_{ref} is the rate constant of the OH + TMB reaction taken from Aschmann et al. (2006). The value of k_{ref} is calculated to be 5.02×10^{-11} cm^3 molecule^{-1} s^{-1} in E1 and 4.89×10^{-11} cm^3 molecule^{-1} s^{-1} in E2.
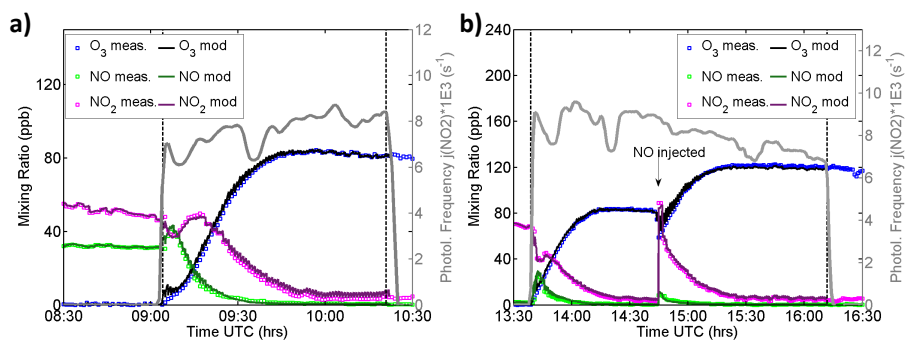
Fig. 1. Measured and modelled time series of O_3, NO_2, and NO mixing ratios in **(a)** experiments E1 and **(b)** experiment E2. The model was constrained by measured O_3, NO_2, and NO concentrations and therefore modelled mixing ratios coincide with measured ones. Photolysis frequency of NO_2 (scaled by 1×10^3) indicated by grey-shaded line. Vertical dashed lines indicate beginning and end of the sunlit experiment.
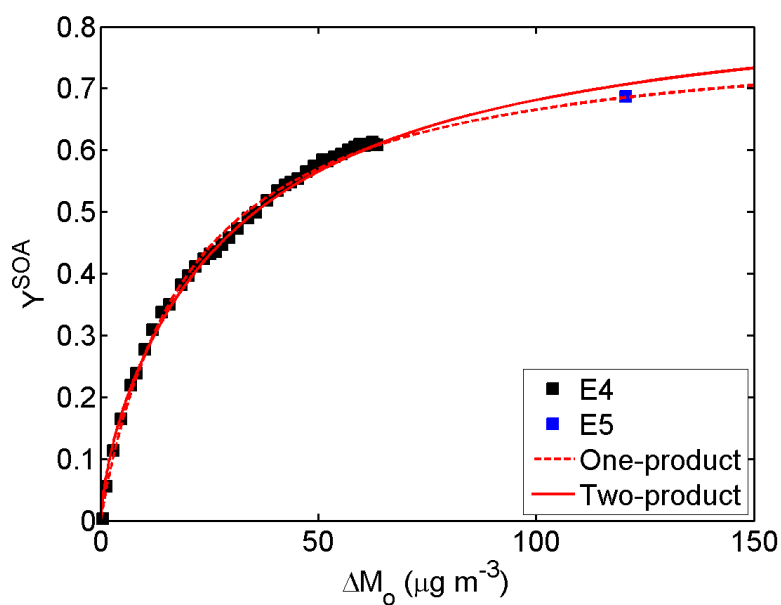
Fig. 2. Secondary organic aerosol yields in the OH-initiated oxidation of MEA as function of organic mass concentration (measured by AMS) in experiment E4 and E5. Data are shown as filled squares. Curves were fitted to the data using the two-product model (solid line) and the one-product model (dashed line). Parameters α_1 and α_2 obtained from the fit are given in Table 4.
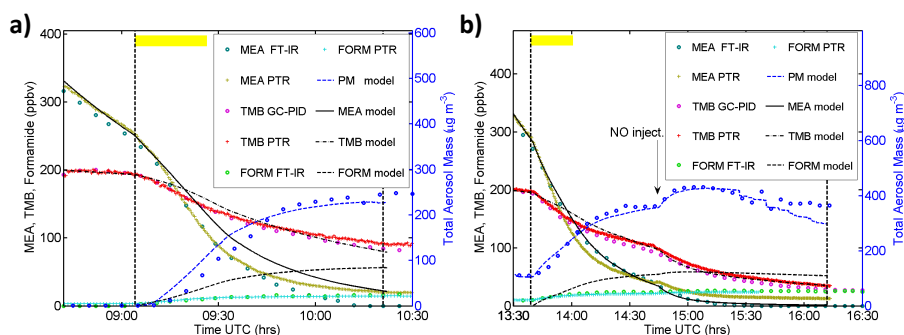
Fig. 3. Measured and modelled time series of MEA, TMB and formamide mixing ratios in **(a)** experiment E1 and **(b)** experiment E2. MEA measurements (golden crosses) from HT-PTR-MS are partly overlaying the MEA data from FT-IR (dark green circles). Measured (blue circles) and modelled (blue dashed line) total aerosol mass concentrations (PM) are in good agreement. Vertical dashed lines indicate beginning and end of the sunlit experiment. Rate constant k_1 was scaled by a factor of 2.6 in the model simulations. Horizontal bar (yellow) marks the time period of the experiment used for the relative rate determination using the LSQ model.

27811
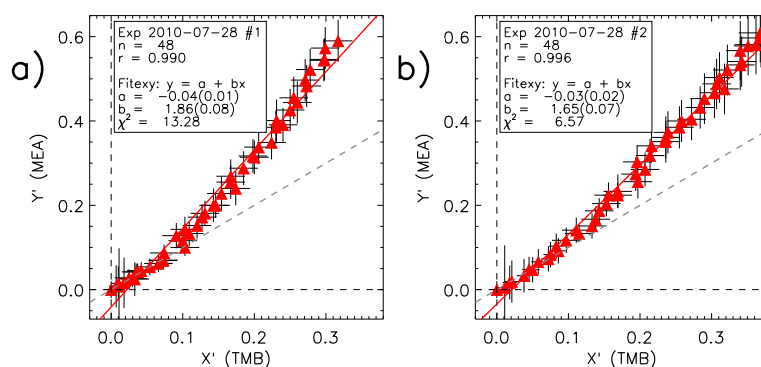
Fig. 4. Results of the fit for X' (horizontal axis) and Y' (vertical axis) according to Equation (19) for **(a)** experiment E1 and **(b)** experiment E2. The experiment period used in the relative rate determination was 1300 s as indicated by horizontal yellow bars in Fig. 2. The result from the least-squares fit (LSQ) is indicated by the straight red line. Fit parameters for E1 are $a = -0.04 \pm 0.01$, $b = 1.86 \pm 0.08$, $\chi^2 = 13.28$ and for E2 are $a = -0.03 \pm 0.02$, $b = 1.65 \pm 0.07$, $\chi^2 = 6.57$. The grey dashed line represents the 1:1 line. The error bars indicate 1-σ statistical errors of both X' and Y' and these errors include measurement errors of TMB (for X') and MEA (for Y') mixing ratios and estimated errors of loss rates L and D_{SF_6}.
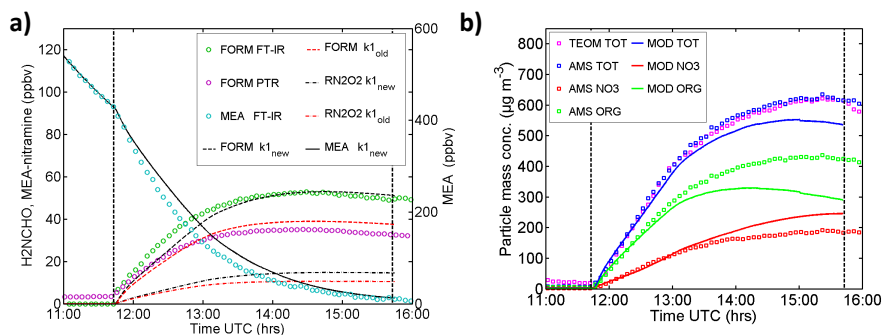
27812

Fig. 5. Concentration time series of experiment E3 on 27 July 2010: **(a)** measured gas phase concentrations of MEA (FT-IR), formamide (FT-IR and PTR-TOF-MS) and modelled formamide (FORM) and nitramine (RN_2O_2) concentrations using the $k(OH + MEA)$ value from EPI Suite v4.0 (red lines) and the value derived in this work (black lines), **(b)** measured and modelled mass concentrations of nitrate (NO_3), high-molecular weight organics $>m/z$ 65 (ORG), and total (TOT) particles. Measured total particle mass data from AMS (blue squares) and TEOM (magenta squares) are in agreement. Nitramine concentrations are scaled by a factor of 5 for better visibility. Vertical dashed lines indicate beginning and end of the sunlit experiment.
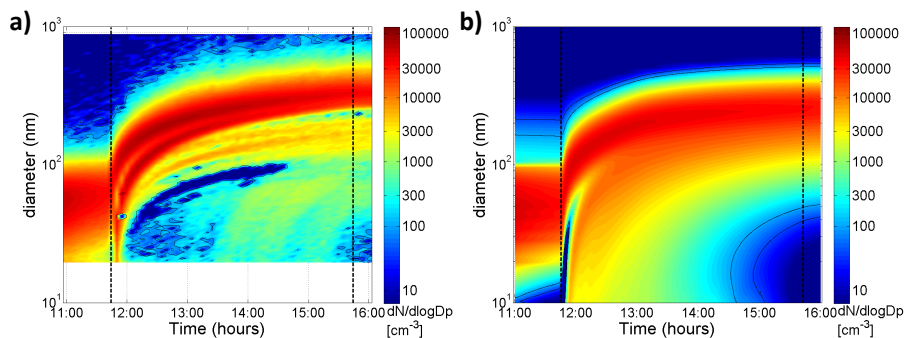
27813

Fig. 6. Sequential number size distribution ($dN/d\log D_p$ in # cm^{-3}) during experiment E3 **(a)** recorded by the SMPS, **(b)** obtained from a simulation with MAFOR. Diameter range shown is from 10 nm to 1000 nm. The lower size cut-off of the SMPS instrument was at 19.5 nm. Vertical black dashed lines indicate beginning and end of the sunlit experiment.